 doi:10.20944/preprints202105.0100.v1

Review

Submerged speleothems and sea level reconstructions: a global overview and new results from the Mediterranean Sea

Fabrizio Antonioli [1]*, Stefano Furlani[2], Paolo Montagna [3], Paolo Stocchi[4,5], Lucio Calcagnile[6,7], Gianluca Quarta[6,7], Jonathan Cecchinel[8], Valeria Lo Presti[9], Maurizio Gasparo Morticelli[10], Franco Foresta Martin[11, 12], Edwige Pons-Branchu[13], Valeria Vaccher[2]

[1] INGV, Roma,via di Vigna Murata 00144, Roma, Italy; fabrizioantonioli2@gmail.com
[2] Department of Mathematics and Geosciences, University of Trieste; via Weiss 2, 34127 Trieste, sfurlani@units.it
[3] Institute of Polar Sciences (ISP), National Research Council (CNR), Bologna, Italy; paolo.montagna@cnr.it
[4] NIOZ Royal Netherlands Institute for Sea Research, and Utrecht University, Landsdiep 4, 16797 SZ Horntje (Texel), The Netherlands; paolo.stocchi@nioz.nl
[5] I4CCS Institute for Climate Change Solutions, University of Urbino, Italy
[6] CEDAD (Centre for Applied Physics, Dating and Diagnostics)-Dept. of Mathematics and Physics "Ennio de Giorgi", University of Salento, Lecce, Italy
[7] INFN (Italian National Institute for Nuclear Physics), Lecce Section
[8]Ustica Diving Center, Piazza Umberto I , Ustica (PA) 90051,Italy;
[9]Studio Tecnico, via Montepellegrino 163, 90142 Palermo, Italy; valeria.lopresti@gmail.com
[10]Dipartimento di Scienze della Terra e del Mare, Università di Palermo, Italy
[11] Laboratorio Museo di Scienze della Terra Isola di Ustica, Rocca della Falconiera, 90051, Ustica (Palermo), Italy
[12] Istituto Nazionale di Geofisica e Vulcanologia (INGV), Sezione di Palermo, via Ugo La Malfa 153, 90146, Palermo, Italy
[13] Laboratoire des Sciences du Climat et de l'Environnement LSCE/IPSL, CEACNRS-UVSQ, Université Paris-Saclay, Avenue de la Terrasse, Gif-sur-Yvette, Île-de-France, 91198, France; Edwige.Pons-Branchu@lsce.ipsl.fr

*Correspondence: fabrizioantonioli2@gmail.com (F.A.)

Abstract: This study presents a global overview of the submerged speleothems used to reconstruct paleo sea level and reports new results from two stalactites collected in the Mediterranean Sea. Coastal cave deposits significantly contributed to the understanding of the global and regional sea level variations during the Middle and Late Quaternary. The studied speleothems cover the last 1.4 Myr and are focused mainly on Marine Isotope Stages (MIS) 1, 2, 3, 5.1, 5.3, 5.5, 7.1, 7.2, 7.3 and 7.5. Results indicate that submerged speleothems represent extraordinary archives providing detailed information on former sea level changes. The two stalactites collected in the central Mediterranean Sea, at Favignana and Ustica islands (Sicily, Italy) are both characterized by continental, phreatic or marine layers. The U-Th and ^{14}C ages of the new speleothems provide results of great interest for relative sea level changes over the last 1000 years.

Keywords: submerged speleothem, phreatic speleothem, sea level change, sea caves, vertical tectonic movements, Ustica, Favignana.

1. Introduction

Preprints (www.preprints.org) | NOT PEER-REVIEWED | Posted: 6 May 2021 doi:10.20944/preprints202105.0100.v1

The study of submerged speleothems in coastal caves significantly contributed to constrain past sea level variations for the last 1.4 Myr, especially for the climatically-important Marine Isotope Stages (MIS) 1, 2, 3, 5.1, 5.3, 5.5, 6.5, 7.1, 7.2, 7.3 and 7.5. Submerged speleothems can be dated using the U-series disequilibrium methods that provide precise and accurate age determination [e.g. 1–5]. These carbonate deposits are usually found in caves that are below the sea level and presently flooded and they often contain marine layers/encrustations or growth hiatuses that identify periods of highstands when the seawater invaded the cave and reached the speleothem.

In addition to speleothems, other biological-physical markers have been used to reconstruct past sea level variations, including shallow-water corals, lagoonal and marine cores, tidal notches and archaeological remains that are well connected with sea level fluctuations. However, most of these indicators suffer of large uncertainties in the age determination due to sample alteration and/or in absolute elevations (e.g. paleowater depth for corals).

Three types of sub, **FFigure 1** Overview map of the Mediterranean region showing the locations (red dots) of the submerged caves discussed in Antonioli et al., 2021. Yellow dots indicate the new sites Favignana and Ustica.

Submerged speleothems have been studied so far: 1) continental (vadose) carbonates (in few cases containing hiatuses), 2) speleothems with overgrowth(s) of marine organisms (e.g. the marine polychaete worm ***Serpula massiliensis***, bryozoans and sponges), and 3) speleothems with phreatic overgrowth(s). The general features of these carbonate cave deposits are described in [6]. In the Mediterranean Sea, more than 300 submerged speleothems were sampled in 32 caves and more than half were analysed for paleo sea level reconstructions [6] (Figure 1). Other speleothem-based sea level records come from few sites in the Caribbean region (Yucatán Peninsula and Cuba), Bahamas, Bermuda and Japan (Minami Daitō island) (Figure 2 and 3), which show very different geological and stratigraphic structures.

Here we provide a comprehensive review of published sea level reconstructions based on submerged speleothems and present new data from two stalactites collected in the Ustica and Favignana Islands in the central Mediterranean Sea. Published data for the Mediterranean Sea have been recently summarized in [6]. Among the most important findings of speleothems retrieved from flooded coastal caves worldwide and often showing hiatuses or marine overgrowths, a special attention deserves the submerged cave deposits from Bahamas [3,4,7], Bermuda [8,9], Yucatan Peninsula [10,11], Cuba [12], and Japan [13]. [14,15] provided an exhaustive review on the use of sea-level indicators preserved in coastal caves, including speleothems and cave sedimentary deposits.

Preprints (www.preprints.org) | NOT PEER-REVIEWED | Posted: 6 May 2021 doi:10.20944/preprints202105.0100.v1

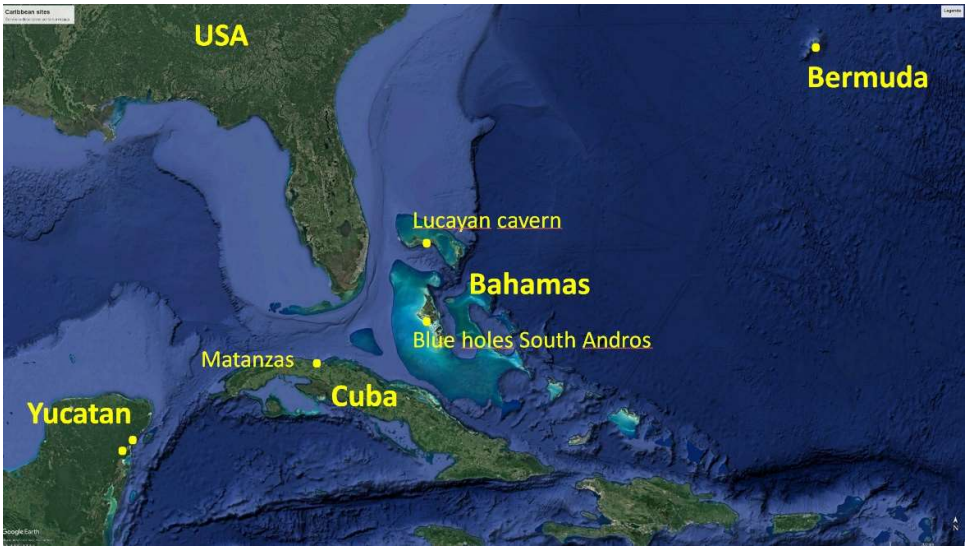

Figure 2 Overview map of the Caribbean region showing the locations of the submerged caves or cenote, discussed in this study. Specific information (latitude, longitude, sampling depths, dating method, ages) are reported in Tables 1.

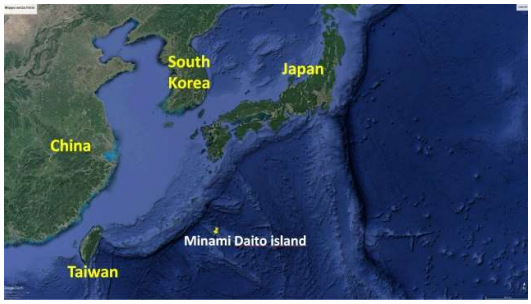

Preprints (www.preprints.org) | NOT PEER-REVIEWED | Posted: 6 May 2021 doi:10.20944/preprints202105.0100.v1

Figure 3a and b Map of the Minami Daito island (Japan). Specific information (latitude, longitude, sampling depths, dating method, ages) are reported in Table 1.

2. Materials and Methods

2.1 Western North Atlantic-Caribbean region and Northern Philippine Sea

Sea level reconstructions based on vadose speleothems and marine overgrowths from the Yucatán Peninsula have been obtained by [10,11], through the analysis of samples collected at elevations between +1.5 and -15.1 m. The Yucatán Peninsula is located in the southeastern Mexico and separates the Caribbean Sea from the Gulf of Mexico. It is almost entirely composed of carbonate and soluble rocks, being mostly limestone although dolomite and evaporites are also present at various depths [16]. The whole Yucatán Peninsula is an unconfined flat lying karst landscape. Sinkholes, locally known as cenotes, are widespread in the northern lowlands [17]. The samples studied by [10,11] formed within Plio-Pleistocene reef and back-reef limestones in a tectonically stable area with little deformation [18].

Phreatic overgrowths and speleothems from Santa Catalina Cave on the northern coast of Cuba were investigated by [12,19]. This cave is carved into Late Pliocene-Early Pleistocene reef limestones [20] and hosts a variety of normal and exotic speleothems, including the mushroom-shaped speleothems, that precisely mark the water level.

Several speleothems and flowstones were studied by [3,4] in the Bahamas islands for past sea level reconstruction. The Bahamas islands include aeolian sands and limestone built on the basement rock of the Florida-Bahamas Platform and are considered a quasi stable area with a low subsidence rate (5 m/100 kyr) [3,21].

Speleothems and marine aragonite overgrowths were analysed by [8,9] in Bermuda. This volcanic seamount is located in the central-western Atlantic and has a carbonate cap with eolian limestone interbedded with paleosol layers. The island's volcanic basement rock is relatively shallow (75 m bsl) and includes 700 m of tholeiitic lavas aged 33 million years. The oceanic crust around the island is about 120 million years old. Bermuda is considered a tectonically stable island but a “near field” with respect to the forbulge ice [22].

Phreatic overgrowths on speleothems (POS) were studied by [13] in the Minami Daito island in Japan (Northern Philippine Sea) to reconstruct Holocene sea level variations. The island is formed as an atoll in the mid-Eocene (ca. 42 Ma ago) on a subsiding volcanic edifice [23] and experienced an average uplift rate of ca. 5 cm/kyr for the last 125 kyr. Based on fossil tidal notches and dated corals the island is considerd stable [24].

Table 1 reports the basic information of the cave deposits from the Western North Atlantic-Caribbean region and Minami Daito island the discussed in the present review. For further information regarding the cave morphology, sampling method, date of sampling and the error associated to the radiocarbon and U-Th ages, the reader should refer to the original publications [3–5,10–13,19,25–38].

2.2 Mediterranean region

The coastline in the Mediterranean Sea (MS) extends for about 46,000 km, with approximately half of it being rocky and characterized by plunging cliffs, sloping coasts,

 doi:10.20944/preprints202105.0100.v1

screes and shore platforms [39]. The MS experiences warm and dry summers and mild and rainy winters owing to its geographic position at the boundary between the subtropical and mid-latitudes zones [40]. It is a highly evaporative basin that is connected with the Atlantic Ocean through the Strait of Gibraltar (sill depth ~ 300 m) and with the Black Sea through the Strait of Dardanelles (sill depth ~100 m) and the Bosphorus Strait (sill depth ~65 m). The coastal geometry and bathymetry of the MS, together with the weather conditions, strongly control the tidal amplitude that varies from place to place along the Mediterranean coasts. The average tidal amplitude is about 40 cm, with the exception of the large tides in the Gulf of Gabes (Tunisia) and in some areas of the North Adriatic Sea where they may reach amplitudes up to 1.80 m. However, in general, the Mediterranean tides have lower amplitudes compared to the other oceanic basins Figure 1.

2.3 Ustica Island

The Ustica Island (central MS, Figure 1) represents the emerged part of a submarine volcano that rises more than 2200 m from the bottom of the southern Tyrrhenian Sea and lies on a deformed continental crust (15-20 km; [41]) along the Africa-Europe plate boundary [42]. The island is located ca. 60 km north of Palermo (northwestern Sicily coast) and covers an area of 8,6 km^2, reaching a maximum elevation of 248 m a.s.l. The structural pattern of Ustica Island and its offshore is characterized by ENE–WSW and N–S-directed extensional and compressional fault systems [42–44]. Ustica island is made up of alkali-basaltic to trachytic composition lava flow and pyroclastic products [45–49] locally covered by marine and continental sedimentary deposits [50]. The present morphology of the Ustica Island and its offshore is the result of the prolonged interplay between volcanic, tectonic and eustatic processes [42,51] active since the Pleistocene and which contributed to the birth of the island occurred between 750 and 130 ky as dimostrated by stratigraphic and geochronological studies corried out on the exposed rocks [49,52].

During the Ustica Island volcanic history, there have been several overlapping cycles of marine ingression and regression, resulting from Middle-Upper Pleistocene glacio-eustatic movements. The sea-level stands related to these oscillations generated typical sedimentary terraces and submerged plains [42,51] which were later uplifted by tectonics at variable height from their original position. Five orders of level surfaces have been identified at heights ranging from about 100 m asl for the oldest and highest terrace, to 5 m asl for the most recent and lowest one [49,53]. The occurrence of marine terraces of variable age at decreasing elevation from the oldest to the youngest, helps in defining the amount of uplift recorded by the island, which has to have been no more than 120 m, at least since the formation of the oldest level surface, that is 350 ka [49,53].

Regarding the geological long term vertical movements, the maximum elevation of MIS 5.5 is 33 m [52] with an uplift rate of 0.21 mm/yr. The recent discovery of fossil barnacle (*Chtamalus*) bands radiocarbon dated to 1823 ± 104 yr AD and covered by a flowstone dated to 1894 ± 24 yr AD in the Grotta Segreta [51], reveals a cosismic event. An uplift of at least 40 cm is suggested that might be related to the strong earthquake in 1906, which obliged all the people to leave the island. This example advises against the use of instrumental data alone for the long-term projections of future sea level rise by 2100 (e.g. GPS data do not reveal vertical movements at Ustica).

2.4 Favignana Island

Preprints (www.preprints.org) | NOT PEER-REVIEWED | Posted: 6 May 2021 doi:10.20944/preprints202105.0100.v1

Favignana (Egadi archipelago, Figure 1) is the closest island to Sicily. The archipelago are formed by carbonate and terrigenous Meso-Cenozoic deposits pertaining to different palaeogeographical domains, covered by unconformable Plio-Quaternary pelagites and clastics. MIS 5.5 calcarenite and biorudite outcrops [54,55] are widely distributed in the eastern sector of Favignana, from 5 up to 10 m [56]. Favignana and the Egadi

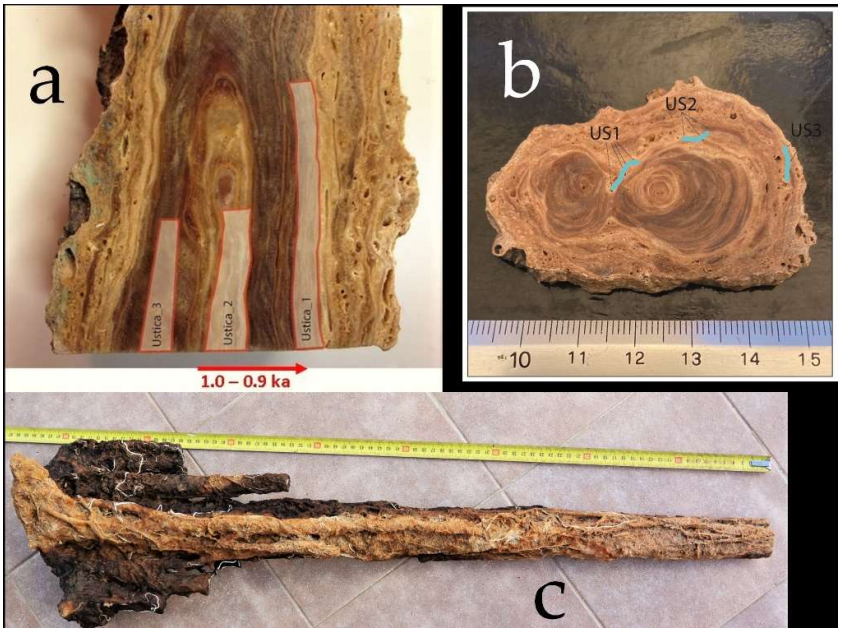

Figure 4 The stalactite sampled at Ustica. a) longitudinal section with sampling area of U\Th ages, refer to Table 2. b) horizontal section with radiocarbon ages, samples US1, US2. US3, refer to Table 3. c) the stalagmite sampled.

Islands may be considered as a stable or slightly uplifted area at least for the last 125 kyr [57–59]. Many outcrops of polygenic conglomerates contain fossil shells of Senegalese

Preprints (www.preprints.org) | NOT PEER-REVIEWED | Posted: 6 May 2021 doi:10.20944/preprints202105.0100.v1

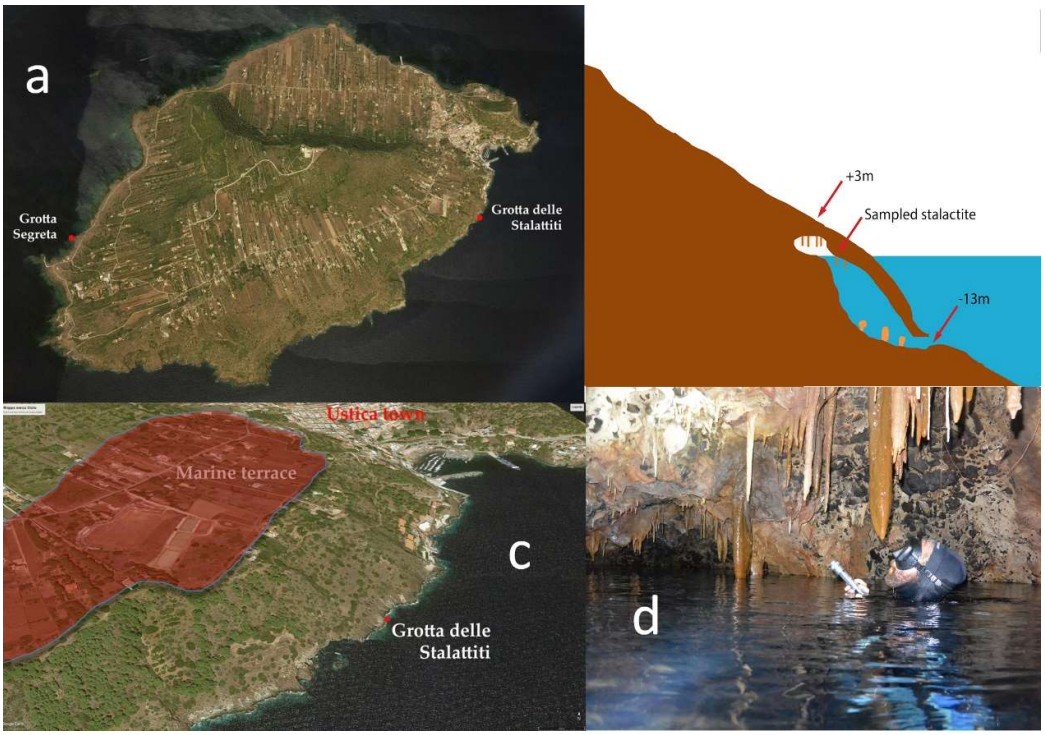

Figure 5 a: Ustica and the location of the Stalactiti and Grotta Segreta caves. b: section of the Stalattiti cave. c: particular of the ubication of Stalattiti cave, Ustica town, and a well carved marine terrace aged MIS 9 [53]. d: into the cave, the sampling area, at sea level in an air bubble.

fauna including *Persistrombus latus* (previously *Strombus bubonius*). Uplifed Middle Pleistocene (MIS 9-11) forms and deposits reach an elevation of 40 m [56].

Preprints (www.preprints.org) | NOT PEER-REVIEWED | Posted: 6 May 2021 doi:10.20944/preprints202105.0100.v1

2.5 Speleothem sampling in Favignana and Ustica

A partly submerged stalactite was collected in 2016 in the Stalattiti cave (Figure 1, 4) on the Ustica island (about 1.4 km from the harbor Figure 5) using a hammer. At the time of the sampling, the deepest portion of the speleothem was 40 cm below the sea level. Elevation measurements were corrected for tide and pressure in order to relate them to the mean sea level (MSL), by using data from the tide gauges of Palermo (www.wxtide32.com) and from the meteorological website www.wunderground.com. The correction was 7 cm for a 1019 hPa pressure. The uncertainty on the elevation measurements of the partly submerged speleothem relative to the sea level, which is on the order of few centimeters, can be considered negligible, even though large uncertainties may arise from the assumed sea level position of markers (Table 1).

A partly submerged stalactite was retrieved in 2014 in the Stalattiti cave (Figure 1, 6) on the NE coast of Favignana island using a hammer. At the time of the sampling, the deepest portion of the speleothem was 30 cm below the sea level. Elevation measurements were corrected for tide and pressure in order to relate them to the mean sea level (MSL), by using data from the tide gauges of Marsala (www.wxtide32.com) and from the meteorological website www.wunderground.com. The correction was 2 cm for a pressure of 1015 hPa.

The uncertainty on the elevation measurements of the partly submerged speleothem relative to the sea level, which is on the order of few centimeters, can be considered negligible, even though large uncertainties may arise from the assumed sea level position of markers (Table 1).

Figure 6 Section of the stalactite sampled at Favignana; 1): continental portion sedimented during MIS 2 (Table 2); 2): the area highlighted in green contains a narrow (3-4 mm) band of marine deposition (Serpulids); 3): the final portion of the speleothem is composed by a stratified white carbonate, typical of phreatic deposition.

 doi:10.20944/preprints202105.0100.v1

2.7 U-Th and ^{14}C dating

Three fragments of spelean calcite were collected within the vadose portion of the stalactite from Ustica (Figures 4, 5) and analysed through the U-series disequilibrium method to determine their absolute age. The fragments were carefully cleaned using a small diamond blade to remove any visible contamination and dissolved with diluted HCl before being mixed with known concentrations of ^{229}Th, ^{233}U and ^{236}U, calibrated against a Harwell Uraninite solution (HU-1) assumed to be at secular equilibrium. The uranium and thorium fractions were separated using UTEVA resin (Eichrom Technologies, USA) and analysed by standard-sample bracketing using a Thermo Scientific Neptune^{Plus} multi-collector inductively coupled plasma-mass spectrometer at the Laboratoire des Sciences du Climat et de l'Environnement (LSCE) (Gif-sur-Yvette) following the protocol developed at LSCE [60]. The $^{230}Th/U$ ages were calculated from measured atomic ratios through iterative age estimation [61], using the ^{230}Th, ^{234}U and ^{238}U decay constants of [62] and [63]. A correction was applied for the non-radiogenic (detrital) ^{230}Th fraction using an initial $^{230}Th/^{232}Th$ activity ratio of 1.5 ± 0.75. However, due to the low ^{232}Th concentration (< 0.05 ng/g) and high $^{230}Th/^{232}Th$ ratio (> 700), the detrital correction has a negligible effect (Table 2).

 doi:10.20944/preprints202105.0100.v1

Site	Coordinates (Lat °N, Long °E)	Sample name	Reference	Dating method	Time range (kyr BP)	Depth (m)	Local tide (m)
Yucatán Peninsula	20.215 -87.4094	Y01-7-2(S) Y01-10-2(S) Y01-22-1(F) Y01-23-2(F)	Moseley et al. (2013)	U-Th (MC-ICPMS)	86.6-61.3 109.2-107.7 hiatus 75.8-70.9 95.3-68.9 115.2-93.8	-14.6 -11 -11 -11 -9.9 -4.9	0.3
Yucatán Peninsula	20.215 -87.4094		Moseley et al. (2015)	U-Th (MC-ICPMS)	Marine: 8.9, 8.6, 8.4, 6 Cont.: 10.9, 8.4, 7.2, 5.8	-6	0.3
Bermuda	32.300 -64.7331	QB	Wainer et al. (2017)	U-Th (MC-ICPMS)	68 -146 79-75 (hiatus) 84-82 (hiatus) 105-92 (hiatus) 137-114 (hiatus)	+1.5	1.35
Japan (Minami Daito Island)	25.8440 131.2301	-	Miklavič et al. (2018)	^{14}C-AMS	5.1-4.6	-0.35	1.5
Cuba, Matanzas (Cueva de Santa Catalina)	23.0859 -81.4184	-	De Waele et al. (2016, 2018)	U-Th (MC-ICPMS)	MIS 11, MIS 9, MIS 7, MIS 5 75.2-363.5	+16	1.08
Bahamas Lucayan Caverns	26.13029 -77.17577	Flowstone DWBAH	Li et al. (1989) Lundberg and Ford (1994)	U-Th (TIMS)	38.8-337.5 5 marine hiati	-15, -10	1.3
Bahamas Grand Bahamas South Andros. Sagittarius flowstone	24.1502 -77.7821	GB-89-25-5	Richards et al. (1994)	U-Th (TIMS)	23.9-79.7; hiatus between 63.7 and 58.5. Tectonic was not considered	-18.1	1.35

 doi:10.20944/preprints202105.0100.v1

Table1

Locations and geographic coordinates of the caves and speleothems reported in this study, with information on references, dating method, time range, elevation, local tide (https://www.tide-forecast.com/)

Preprints (www.preprints.org) | NOT PEER-REVIEWED | Posted: 6 May 2021 doi:10.20944/preprints202105.0100.v1

Sample	[^{238}U] (μg/g)	[^{232}Th] (ng/g)	$\delta^{234}U_m$ (‰)	$(^{230}Th/^{238}U)_{act}$	$(^{230}Th/^{232}Th)_{act}$	Age (kyr)	Age $_{corr}$ (kyr BP)*
Ustica-1	1.194 (0.001)	0.0483 (0.0005)	67.4 (0.6)	0.00939 (0.00007)	702.7 (5.4)	0.97 (0.01)	0.89 (0.01)
Ustica-2	1.143 (0.001)	0.0340 (0.0004)	67.5 (0.8)	0.01024 (0.00023)	1041.5 (24.0)	1.05 (0.03)	0.98 (0.03)
Ustica-3	1.543 (0.002)	0.0236 (0.0005)	70.5 (0.9)	0.00989 (0.00021)	1944.3 (42.3)	1.01 (0.02)	0.95 (0.02)

Table 2 Results of the U/Th dating of the vadose speleothem (Ustica 1, 2, 3, Figure 5. ^{238}U and ^{232}Th concentrations were determined using the enriched ^{236}U and ^{229}Th isotopes, respectively. $\delta^{234}U_m = \{[(^{234}U/^{238}U)_{sample}/(^{234}U/^{238}U)_{eq}]-1\} \times 1000$, where $(^{234}U/^{238}U)_{sample}$ is the measured atomic ratio and $(^{234}U/^{238}U)_{eq}$ is the atomic ratio at secular equilibrium.$\delta^{234}U_{(0)}$ corr is the initial value and is calculated by the equation:$\delta^{234}U_{(0)} = \delta^{234}U_m \exp(\delta_{234}t)$, where t is the corrected age in years and δ_{234} is the decay constant for ^{234}U. * Ages corrected for detrital ^{230}Th using an inital ^{230}Th/^{232}Th activity ratio of 0.85 ± 0.36 [64].

1 Sample	2 Corrected Altitude (cm)	3 Radiocarbon Age (BP)	4 δ^{13}C (‰)	5 Kind of markers	6 Cal BP 1 Sigma
LTL15761A	-32 ± 5	1912 ± 45	+2 ± 0.7	S2 serpulids	1485-1304 1395±45
LTL15762A	-35 ± 15	806 ± 45	+3 ± 0.5	S3 phreatic	735-675 705±30
LTL15762B	-32 ± 5	19886+/-100	-29.5 ± 0.5	S1 continental	24013-23795 23.903±109
R – 2741*	-30 ± 10	531 ± 32	+1.40*	Cala Mancina St Vito Lo Capo	232 – 106 169±63
R – 2742*	-30 ± 10	527 ± 36	+1.33*	Cala Mancina St Vito Lo Capo (Tp)	232 -94 163±69
R – 2764*	-30 ± 10	554 ± 35	+1.31*	Calazza (Pa)	251 – 127 189±62
R – 2580*	-40 ± 10	784 ± 37	+1.76*	Barcarello (Pa)	412 -146 279±133

Table 3 Radiocarbon data Favignana stalactite cave, Column 1: the Lab. Number * from **[65]**. 2: Corrected altitude of samples; 3: radiocarbon age; 4) δ^{13}C (‰) *unavaialable error bar; 5) kind of markers used for the radiocarbon analysis; 6)The obtained conventional radiocarbon ages were calibrated by using the Calib 8.10 software **[66]**

Radiocarbon dating for the Ustica and Favignana samples was carried out at CEDAD-Centre for Applied Physics, Dating and Diagnostics at the University of Salento, [67]. The selected samples were carefully removed from the matrix by using a diamond blade. The extracted portion of the sample were then analyzed at the optical microscope in order to identify and mechanically remove adering particles or unwanted farction of the matrix. The sample were then attacked with H_2O_2 in order to remove the uppermost

Preprints (www.preprints.org) | NOT PEER-REVIEWED | Posted: 6 May 2021 doi:10.20944/preprints202105.0100.v1

layer and then hydrolised under vacuum to CO_2 by usign HCl. Extracted CO_2 was then catalitically reduced to graphite which was then used to measure the radiocarbon age by AMS (Accelerator Mass Spectrometry). The radiocarbon dating beamline was used, based on a 3MV Tandetron accelerator (Mod. HVEE 4130HC) to measure the radiocarbon content. After correction for machine and processing background the conventional radiocarbon age of the samples was calculated. For continental samples conventional radiocarbon ages were calibrated by using the INTCAL20 calibration curve while marine samples were calibrated by using the MARINE20 [68] curve and a local ΔR=-88±50 yrs [69] Table 4 Figure 5.

Campione in sezione	Campione	Radiocarbon Age (BP)	δ13C (‰)	Note
1	LTL20043A	2231 ± 45	-18.3 ± 0.6	US1
2	LTL20044A	1954 ± 45	-17.1 ± 0.7	US2
3	LTL20045A	1929 ± 45	-23.7 ± 0.4	US3

Table 4 Radiocarbon data of the outer overgrowth of Ustica stalactite, column 2): the Lab. Number; column 3): radiocarbon age; column 4): $\delta^{13}C$ (‰); column 5): the sample as named in Figure 5b.

2.8. Numerical modelling of glacial- and hydro-isostatic adjustment and sea-level change

Land-based sea-level indicators such as speleothems, keep track of past sea-level changes that are referenced to the surface of the solid Earth. Because the latter can be affected by vertical motions, the recorded sea-level fluctuations in speleothems are defined as local Relative Sea Level changes (RSL).

In particular, ice-driven sea-level changes stem for the contribution of ocean mass variations (in response to continental ice mass variations) as well as solid Earth deformations and vertical geoid perturbations [70–72]. In fact, when water mass is transferred from ice sheets to oceans, and viceversa, solid Earth deforms in order to restore the isostatic equilibrium under a different surface loading setting. Solid Earth deformations and ice masses, then, behave as density anomalies, thus affecting the vertical position of the mean sea surface, which is an equipotential surface of gravity (geoid). This process, which is known as glacial- and hydro-isostatic adjustment (GIA), is responsible for regionally-varying RSL changes that are modulated in time the the viscous flow of the Mantle material.

Because of mass conservation, the ocean averaged RSL change corresponds to the global mean, or eustatic, sea-level change. Based on the geographical distance from the ice sheets, the local RSL change can be very closte to the eustatic (ice distal o far-field regions), or significantly different, if not opposed to the eustatic (ice proximal areas). The largest deviations from the eustatic signal are found where ice sheets grow and shrink. In particular, during glacial perionds and underneath the growing ice sheets, the crust subsides and forces the upper mantle material to flow outwards, thus causing the uplift of the ice-proximal peripheral area that forms the so-called forebulge. Between the forebulge and the ice margins, the local RSL rises due to the crustal subsidence and the geoid uplift that is caused by the gravitational pull that the ice masses exert on the ocean water. On the other hand, on top of the forebulge, the local RSL drop is much larger than the eustatic during glacial periods because of the combination of crustal uplift and geoid subsidence. When the ice sheets melt, the ice-covered areas undergo uplift, while the forebulge ares experience a strong subsidence that, combined to the eustatic signal, results in a much higher-than-average RSL rise. The vertical motions that affect the

Preprints (www.preprints.org) | NOT PEER-REVIEWED | Posted: 6 May 2021 doi:10.20944/preprints202105.0100.v1

forebulge areas are not just relevant for the ice proximal location, but also for the far-field equatiorial and continental coastal areas. Here, in fact, despite the distance from the ice sheets, the RSL changes that follow major deglaciations may strongly deviate from the eustatic and show up with an opposite sign. In fact, because of mass conservation, ocean water flows towards the subsiding peripheral forebulges, and locally results in a RSL drop that follow an initial highstand. This process is known as ocean syphoning.

Interestingly, some of the Caribbean and Yucatan speleothems, are sitting in areas where the compex forebulge ocean syphoning dynamics operate.

Therefore, RSL indicators provide constraints on past ice-sheets chronologies and on the relevant Earth rheological parameters that regulate deformation of the planet in response to surface ice and water loading.

To compute the local ice-driven relative sea-level changes, the gravitationally self-consistent sea level equation (SLE; 1-4) must be solved for a prescribed ice sheets chronology and Earth rheological model. The SLE is a linear equation that yields, for any variation of land-based (i.e. grounded) ice thickness, the time- and space-dependent vertical deformation of the mean sea surface and of the solid surface of the Earth, the difference of the two being the relative sea-level (RSL) change. We employ SELEN [70–72] to solve the SLE and retrieve the local GIA-modulated RSL curves at each site considered in this paper. The latest, up-to-date version of open source model SELEN includes the rotational feedbacks as well as the form treatment of the time-dependent ocean function (i.e. variable coastlines).

We assume a self-gravitating, rotating, spherically symmetric, radially stratified, deformable but not compressible Earth model. The latter is 1-dimensional and all the relevant rheological parameters depend on the Earth's radius only. The outer shell of the model is perfectly elastic and represents the Lithosphere. Between the Lithosphere and the inviscid Core is the Mantle, which is characterized by linear Maxwell viscoelastic rheology. The mantle can be discretized into a number of layers.

First, we discretize the VM2 mantle viscosity profile [73] over a four-layer model where the upper mantle (UM), the lower upper mantle (LUM), the transition zone (TZ) and the lower mantle (LM) are characterized by a Maxwell viscoelastic rheology and laterally uniform viscosity (see Table 5). We combine this with a lithosphere thickness of 90 km. We use this as a reference model to be combined with three ice sheets chronologies.

VM2	LT (km)	UM (x 10^{21} Pa·s)	LUM (x 10^{21} Pa·s)	TZ (x 10^{21} Pa·s)	LM (x 10^{21} Pa·s)
	90	0.67	0.44	0.46	2.53

Table 5 Elastic lithosphere thickness and viscosity of the four-layer VM2 profile.

MVPs	LT (km)	UM (x 10^{21} Pa·s)	TZ (x 10^{21} Pa·s)	LM (x 10^{21} Pa·s)
MVP1	100	1	1	2
MVP2	100	0.5	0.5	5
MVP3	100	0.25	0.5	10

Table 6 Elastic lithosphere thickness and viscosity of the three-layer MVP 1-3 profiles.

We employ the following ice sheets models:

Preprints (www.preprints.org) | NOT PEER-REVIEWED | Posted: 6 May 2021 doi:10.20944/preprints202105.0100.v1

- ICE-5G [73]: this global model describes the ice-sheet thickness variations over North America, Eurasia, Greenland and Antarctica during the last 123 ka. Geological and modern geodetical observations are used to constrain the ice thickness chronology between 26 ka and present-day [6]. Through an iterative procedure, the SLE is solved for an *a priori* ice sheets configuration and a prescribed fixed solid Earth model (mantle viscosity profile and Lithosphere thickness). The predicted RSL elevations and modern vertical rates are compared to, respectively, paleo RSL indicators and measured crustal and geoidal vertical velocities. The differences between predictions and observations are then used to to modify the ice sheets models until a satisfactory solution is found. The ice sheets volumetric evolution between 123 and 26 ka is tuned to the $\delta^{18}O$ curve [74] and loosely constrained by surface geological evidences that define the ice margins.. Here we combine two ICE-5G chronologies in time in order to cover the time span under consideration and to evaluate the GIA-modulated RSL response to the melting of the MIS 6 ice sheets during the MIS 5e. The latter is characterized by a ~0.9 m eustatic sea-level highstand above present-day msl between 129.5 ka and 123 ka, mostly coming from a reduced (with respect to present-day) Greenland Ice Sheet.

- ICE-6G [75]: this model follows from an improvement of the ICE-5G. Here we apply the same repetition in series of ICE-5G. According to the ICE-6G, the maximum MIS 5.5 eustatic highstand between 129 ka and 123 ka is ~3.1 m above present-day msl as a consequence of reduced Greenland and West Antarctic Ice Sheets

- ANICE-SELEN [76,77]: this global chronology model is the result of an inverse forward modelling procedure where the $\delta^{18}O$ stack [74] is decoupled into global ice sheets volume and deep-water temperature. For this purpose, 3D thermomechanical ice-sheet models for North America, Eurasia, Greenland and Antarctica, are dynamically coupled to SELEN in order to include all the GIA feedbacks. ANICE-SELEN is not yet constrained by geological or instrumental data. Here we use the original ANICE-SELEN chronology, which is characterized by ~2.5 m eustatic highstand during MIS 5 e (125-117 ka), in response to a reduced Greenland Ice Sheet volume.

The temporal volume variations of three ice sheets models between are therefore dependent, to a certain degree, on the benthic oxygen curve [74].

3. Results

We divived the paragraph in two parts, the first one regarding published data in the Western North Atlantic-Caribbean region and Japan (par. 3.1), while the second one regarding new data in the MS (par. 3.2).

3.1 Review data

3.1.1 Bermuda

The Western North Atlantic–Caribbean region, and Bermuda in particular, is strongly affected by the vertical motions of the periglacial forebulge that forms as a result of upper Mantle flow in response to the expansion of the Laurentide ice-sheet during glacial periods.

[9] provided an interesting review that summarized previous literature in the Bermuda area and the NE coast of the USA. The authors also published the results of a new stalactite sampled in a cave at +1.5 m asl in the age range from 137.0 ka to 71 ka. Four hiati are clearly visible in a continuous deposition on the speleothem (Table 1). A first hiatus (MIS 5.5) occurs from 137.0 ka to 114.7 ka, a second hiatus occurs from 105.9 ka to 92.0 ka corresponding to MIS5.3. The third hiatus ranges from 84.3 ka to 82.0 ka and corresponds to MIS5.1, with the presence of an additional hiatus from 79.9 ka to 75.0 ka corresponding to MIS5.1bis.

Preprints (www.preprints.org) | NOT PEER-REVIEWED | Posted: 6 May 2021 doi:10.20944/preprints202105.0100.v1

U-Th age uncertainties range between ±7 ka and ± 1 ka. These data support previous controversial indications that Bermudian RSL was significantly higher than RSL at other locations during MIS5.5 and MIS 5.3 Figure 2, Table 1.

3.1.2.1 Andros island (Bahamas)

[4] sampled and studied 116 speleothems collected from 22 caves which are part of a wide cave systems in Andros island (Bahamas) during several expeditions from 1984 to 1992 (Figure 2, 7).

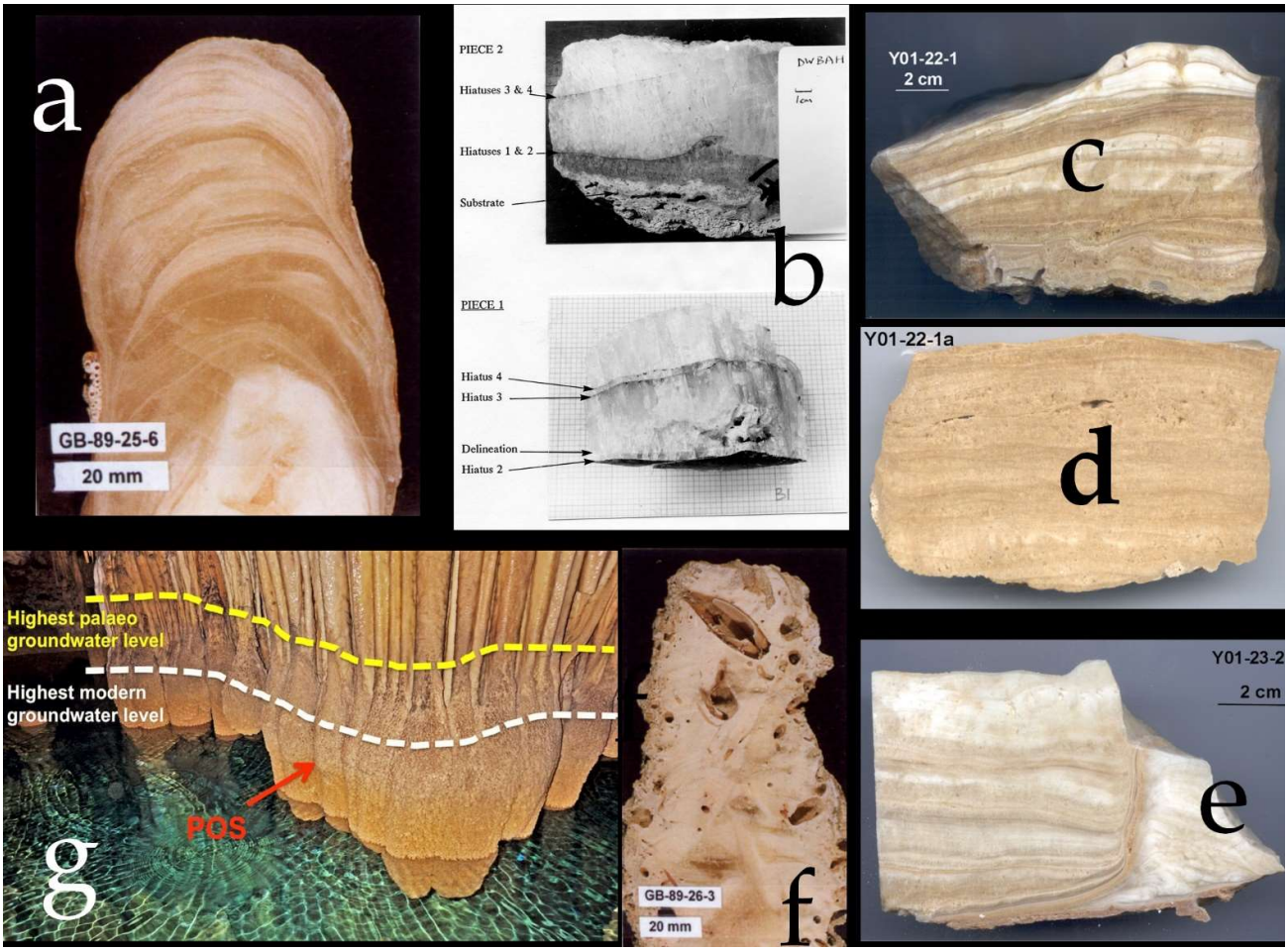

Figure 7 submerged speleothems from Caribbean. a: Bahamas Blue hole, South Andros., stalagmite GB-89-25-6 partially coverd by serpulid overgrowths, -13.8, Lucayan cavern (courtesy David Richards). b: the DWBAH flowstone, sampled at -15 m in the Grand Bahama Island (courtesy Joyce Lundberg). c,d: flowstone Y01-22-1, Y01-22-1a, -9.9, Yucatan (courtesy Gina Moseley). e: flowstone Y01-23-2, -4.9, Yucatan (courtesy Gina Moseley). f: Bahamas Blue hole, South Andros., stalagmite GB-89-26-3 a stalagmite bored by Lithophaga (courtesy David Richards). g: Japan, phreatic speleothem at Minaido Daito island (courtesy Blaz Miklavic).

Table 1 reports the results of one of the most interesting speleothem collected at -18.1 m and covering almost the entire glacial period. The speleothem was sampled from -53.6 m and -13.8 m. Regarding the flowstone sequence, which was calledGB-89-25-5A/ B/ C, at -18.1 m bsl (Table 1, Figures 1 and 2) the authors wrote that "other samples grew continuously throughout this period. We cannot, therefore, support the suggestions for high sea-stand events near present sea level between 93 and 15

Preprints (www.preprints.org) | NOT PEER-REVIEWED | Posted: 6 May 2021 doi:10.20944/preprints202105.0100.v1

kyr". The same speleothem shows a non-erosional hiatus between 63.7± 1.7 kyrs and 58.5±0.7 kyr corresponding to MIS3 (Table 1 Figure 6).

3.1.2.2 Lucayan Cavern DWBAH Flowstone (Bahamas)

This can be considered a historical discovery. The results of the work were published in 1989 using the precise U-Th TIMS dating [3]. After 32 years, it remains one of the most complete sequences: the DWBAH flowstone, sampled at -15 meters in the Lucayan Cavern (Little Bahamas), the flowstone started to form ~ 300 kyr ago at -10 m and ceased its growth ~ 39 kyr ago. The fowstone show 5 hiati in correspondence of MIS9, MIS7.5, MIS7.3, MIS5.5, MIS5.3 (Li et al., 1989, Lundberg and Ford 1994). The tectonic rate considered for the Bahamas area is 1 m every 50 kyrs, as suggested by [7] (Table 1, Figures 2, 7)

3.1.3 Santa Catalina Cave (Cuba)

The Santa Caterina cave is carved in a marine terrace, which occurs along the Cuban coast. [19] suggested a general slowly uplifting trend during the Pleistocene, even if U-Th datings of these terraces are difficult to achieve considering local conditions. The minimum age of the terraces can be constrained by dates carried out onspeleothems from coastal mixing (flank margin) caves formed during past sealevel highstands together with the carving of the marine limestones (Table 1, Figure 2). The authors suggested that speleothems collected in the Santa Catalina Cave (Matanzas) provided ages >360 kyrs and showed several cycles of subaerial–subaqueous corrosion and speleothem growth. This suggests that the cave was carved during the MIS 11 sea-level highstand or earlier. Some stalagmites grew from MIS 11 up to MIS 8 and were submerged twice, once at the end of MIS 11 and then during MIS 9. Phreatic overgrowths (POS) covering the speleothems suggest the presence of anchialine conditions within the cave during MIS 5.5. The alitutde of these speleothems, 16 m asl, indicates a late Pleistocene uplift rate lower than 0.1 mm/kyr.

3.1.4 Yucatan

[11] found and dated 4 marine levels between 8.9, 8.6, 8.4 6 ka cal BP collected on a spectacular stalactite sampled at - 6 meters in a Cenote in the Yucatan Peninsula. He interpreted dated levels as sea level fluctuations: "therefore, it seems highly likely that four relative sea-level 'Oscillation Events are responsible for submergence and re-emergence. These oscillations are presumably due to GIA movements since all the area is considered tectonically stable". Authors also discussed the results obtained by [78] on the U-Th ages from the *Acropora palmata* fossil corals and suggested that the error related to the paleoposition of the sea level can reach 10 m, while a submerged speleothem with marine layers show a centimetric error bars, also considering the local microtidal amplitude of 0.3 m (Table1, Figure 2).

[10] provided an age for numerous speleothems sampled in different submerged caves and Cenotes in the Tulum area (Table 1, Figures 2, 7) at -14.6, -11, -9.9 and -4.9 m. The results summarized in Table 1 allowed the authors to indicate that between 109 kyrs and 61 kyrs the highstand of MIS 5.1 did not reach the lowest altitude of the speleothems studied (-14.9 m bsl). As for the MIS 5.3 highstand, it did not reach an altitude of -11 m bsl. For as regards the MIS 5.5, the precise speleothem age measured at -4.9 m bsl, it provides

Preprints (www.preprints.org) | NOT PEER-REVIEWED | Posted: 6 May 2021 doi:10.20944/preprints202105.0100.v1

a robust chronology for the timing of the fall at the last interglacial termination, or the 5.5-5.4 transition.

3.1.5 Minami Daito Island (Japan)

[13] studied the partially flooded Akiba Chiteiko Cave, in a little atoll, in Northern Philippine Sea (Figure 3). The speleothem shows a phreatic overgrowth on speleotem (POS). Sampling and dating the highest POS level, that corresponds to the high tide mean level (Figure 7), Authors suggest that sea level reached its Holocene maximum highstand between 5.1 and 4.6 ka cal BP, after which it remained more or less stable till the present day, with a possible minor sea-level drawdown of about 35 cm. The SL on Minami Daito did not have a distinct highstand in the Holocene, which coincides with the mid- Holocene maximum observed elsewhere in the Indo-Pacific basin.

3.2 New data

3.2.1 Favignana

In a small cave at Favignana island (Egadi Archipelago, Sicily) we sampled and analized a speleothem with continental, marine and phreatic layers (Figure 4, 5). The cave (Figure 8) entrance is narrow, with a length of 14 m, an average width of about 3-4 m and a depth of about 7 m at the entrance that reduces to about 4 m inwards. The studied speleothem, more precisely a stalactite, was blade-shaped and it was collected at the bottom of the cave. It was about 1 m in width. Today the cave is flooded and the sea level lays 0.35 m above the speleothem. (Table 4).

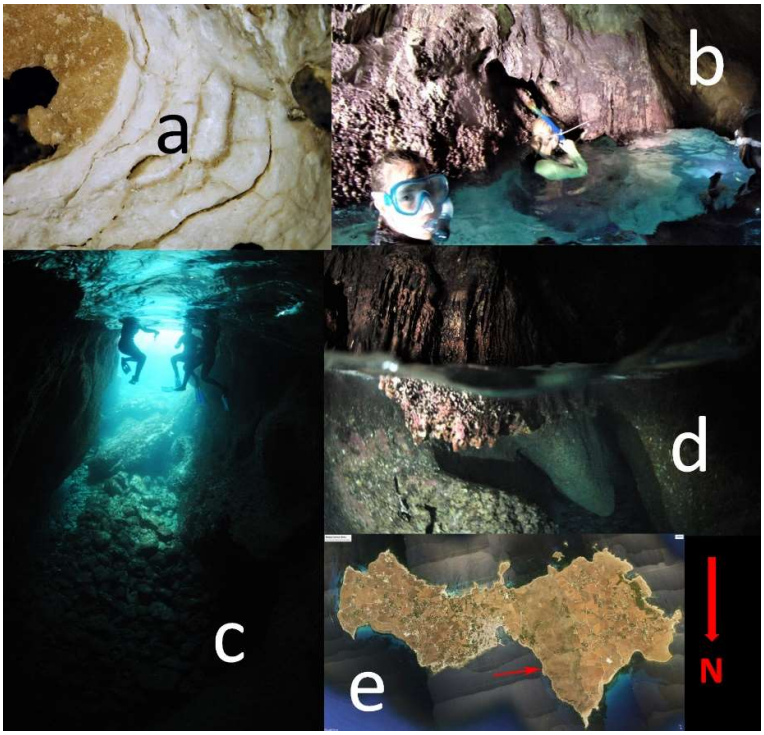

Figure 8 Coastal cave and submerged speleothems at Favignana Italy (Figure 1, 4; Table 2, 3). a: section of stalactite sampled at -0,32 m with the continental portion (brown) and the phreatic portion (white). b: sampling survey at the bottom of the cave. c: photo of the cav.e d: the appearance of the freshly sampled stalactite. e: Favignana and the site of the stalattiti cave.

The speleothem shows an emerged part made of brown coloured subaerial carbonatic facies, and a 6 cm white carbonate facies suggesting a phreatic genesis. Between the aforementioned facies we also noted and analized (Figure 4) a marine overgrowth made up of serpulids. Radiocarbon ages of subaerial carbonatic overgrowth provided an age of 23.9 kyrs cal BP, while the marine overgrowth of 1.3 kyrs cal BP and the last presently submerged phreatic layer provided an age of 0.7 kyrs cal BP.

3.2.2 **Ustica**

The submerged cave (location and sketches in Figure 5) has a small entrance at -13 m bsl. A 10 m x 10 m room with open-air at the sea level was found inward. The cave roof was estimated to be about 2 m in height asl. Hundreds of stalactites hang from the vault of the cave, all formed only of continental carbonate. There are alsosome plant roots. In the submerged portion, both on the cave walls and the submerged stalagmites and stalac

tites, Polychaeta overgrowth can be observed. In some cases, they appear to be very large, up to 7-8 mm in diameter) Figure 4. The stalactite sampled around the present-day sea level is sprinkled with living Polychaeta. Once dissected, it showed (see Figure 4) a dark brown central part due to continental/phreatic deposition occurred in subaerial

Preprints (www.preprints.org) | NOT PEER-REVIEWED | Posted: 6 May 2021 doi:10.20944/preprints202105.0100.v1

environment. On the contrary, microscope analysis show that the external part of the speleothem, made oflighter tones, presents a mix of both marine, with polychaetes and continental origin (Figure 5). The age of this stalactite resulted to be about 1000 years (Table 2). Radiocarbon datings carried out on the outermost part of the speleothem (Table 3), show an older age while maintaining a stratigraphically correct sequence.

3.3 GIA numerical predictions

For the three ice sheets models, the predicted RSL curves computed at each location and for each of the four mantle profiles, tend to be distributed above the eustatic curves, with Japan being the only exception as it is almost continuously below the eustatic

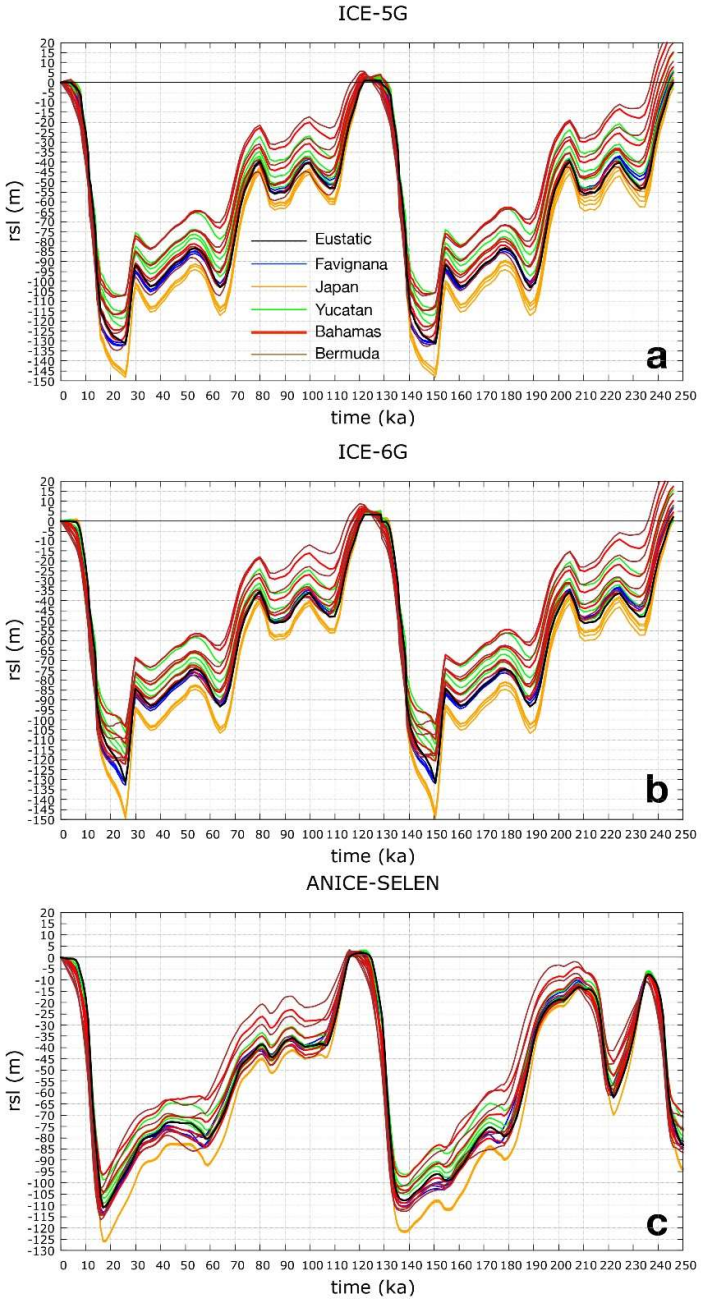

 doi:10.20944/preprints202105.0100.v1

Figure 9 Cumulative predicted RSL curves for ICE-5G (a,d), ICE-6G (b,e) and ANICE-SELEN (c,f) ice sheets models in combination with different mantle viscosity profiles (see legend and Table 5 and 6 for details). The black curves represent the eustatic sea level variation for each ice sheets model. The colored curves represent the RSL change for each site under consideration.

throughout the last 250 ka (Figure 9 a-c). The Mediterranean sites (Ustica and Favignana) are very close to the eustatic component and do not show significant variability as a function of mantle viscosity profiles. The same holds for Japan, where local RSL variability is larger for ICE-5g and ICE-6g and negligible for ANICE-SELEN. In the Caribbean and Yucatan, instead, the local RSL variability is of the order of 20-30 m during glacials and interstadials, and decreases during the MIS 5.5. This implies that Bermuda and Bahamas, being closer to the north American ice sheets margins, are more sensitive to GIA-modulated vertical motions, which can be emphasized by specific viscosity profiles.

RSL predictions vs data (MIS 5.1 – 5.3)

Overall, the predicted RSL peaks are generally lower than the observed terrestrial limiting elevations (deposition) as well as the hiatuses and the marine transgressions inferred from the speleothems (Figure 10). The largest RSL variability is predicted at Bermuda (Figure 9, 10c) because of the relative proximity to the ice sheets margins and peripheral forebulge. Here, though, the maximum predicted highstands at MIS 5.1 and MIS 5.3 are, respectively, ~20 and ~15 m lower than the speleothem elevation. Furthermore, the predicted highstands at MIS 5.1 and 5.3 are, respectively, ~5 and ~13 m

Preprints (www.preprints.org) | NOT PEER-REVIEWED | Posted: 6 May 2021 doi:10.20944/preprints202105.0100.v1

higher than those at Yucatan (Figure 10 b). These differences are in line with the results of [9], but significantly smaller. We argue that this might be related to the very different ice sheets models (ICE-1 and ICE-2) used by [9]. Also, our predictions at Bermuda are only slightly higher than at Bahamas (Figure 10d), implying that both sites share the same GIA response for the three ice sheets models and four mantle viscosity profiles.

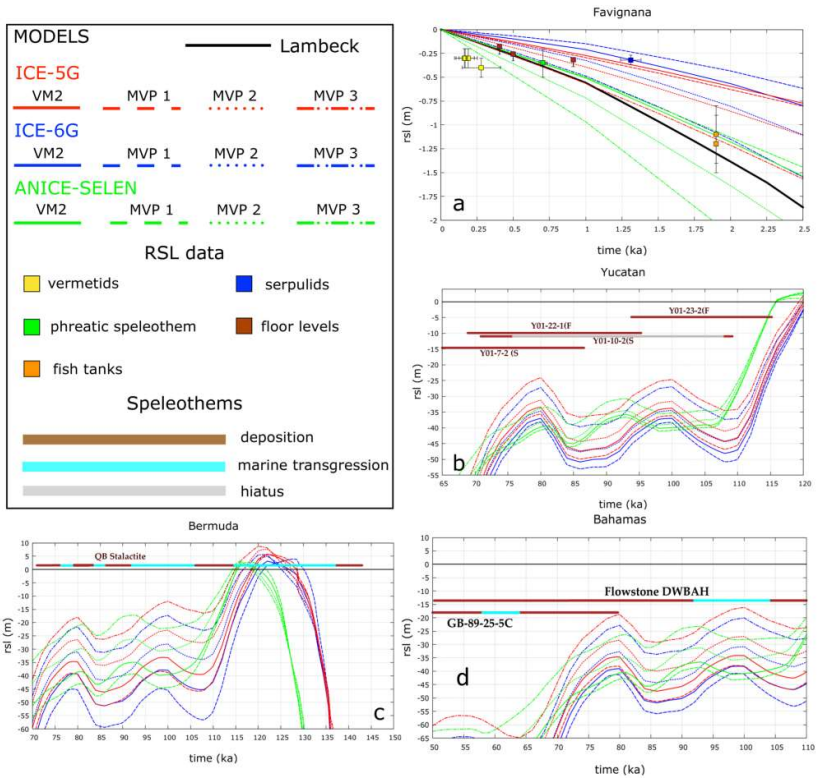

Figure 10 Predicted RSL curves for ICE-5G (red curves), ICE-6G (green curves) and ANICE-SELEN (blue curves) ice sheets models in combination with MVP 1-3 mantle viscosity profiles (solid, dashed and dotted, respectively) at each site and with respect to the measured elevations. a, Favignana. b, Yucatan. c, Bermuda. d, Bahamas.

4. Discussions

Considering data reviewed in the paper and in [6], the use of submerged speleothems provided remarkable results for the global sea level change history during the Holocene and for the long-term sea level change reconstruction, such as during the Late to Middle Pleistocene, in particular for MIS 1, 3, 5.1, 5.3, 7.1, 7.2, 7.3 7.5, MIS 9 highstands (Tables 1, 2 ,3, 4). In particular, figures 11 and 12 depict all the results for the Caribbean and Japan submerged speleothems and some of the main results of the aforementioned review for the Mediterranean area [6] have been compared with the global curve of [79]. In the table 1 presented by [6], a speleothem sampled in Italy (Custonaci) show marine and continental levels and seems to be the older: aged at MIS 25-37 (1.4 MA).

4.1 Favignana stalactite

This speleothem provides an interesting result concerning sea level change for the last 1300 years, due to the fact that sea level data are very scarce in tectonically stable areas of the Mediterranean sea [80,81]. The submerged portion of the stalactite is truncated and bored by *Lithophaga lithophaga*, The cave (Figure 8) could be recently greatly enlarged by marine processes, such as storm waves, also considering the fact that the almost all the other stalactite near the one we have studied are truncated. Therefore we hypothesize the evolution following described:

1) During LGM the sea level was far from here, at about -129 m bsl [82] and the speleothem presumably formed a column (Figure 11) aged 23.9 ka BP (Table 3).

Preprints (www.preprints.org) | NOT PEER-REVIEWED | Posted: 6 May 2021 doi:10.20944/preprints202105.0100.v1

2) sea level rose up until 1395 years cal BP. The sea level stillstand at -0.32 m shows a stillstand which promote the growth of colonies of serpulids and sponges that formed on the broken surface of the speleothem, as reported at the Argentarola cave by [38,83].

3) the following millimetric layer of phreatic carbonate (Figures 11) shows that the aforementioned sea level stillstand was up to -0.35 m, considering the deepr phreatic level,. Radiocarbon datings of the most recent level is 705 kyrs cal BP (Table 3) .

4) the phreatic level was then interrupted by marine ingression, so now the submerged part of the stalactite is bored by *Lithophaga sp.*, while the external carbonatic surface of the submerged part of the speleothem is colonized by small Serpulids, tetracorals, limpets and sponges.

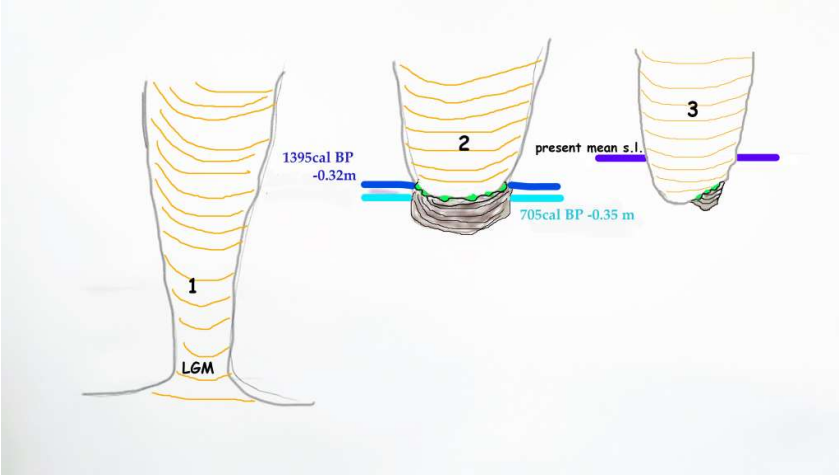

Figure 11 Evolution scheme of the speleothem sampled in the stalactite cave in Favignana. 1: continental deposition during lgm. 2: sea level was 0.35 m lower when a serpulids overgrowth. 3. Present day

The levels of phreatic carbonates have been used in the Mediterranean as sea level markers by [28,30]. In our case, the entire phreatic formation has not been preserved, but only some non-eroded fragments were observed. For this reason we can hypothesize (as happens for the cave from Palma de Mallorca) a thickness of the phreatic deposit (in the shape of a ball) on average as high as the average tide of Favignana (annual mean: 32 cm, OSU tidal prediction model, http://volkov.oce.orst.edu/tides/otps.html), it could also be assumed a greater thickness in depth of the phreatic.

Furthermore, the age correction due to dead carbon is not difficult in this case. It showed that the value of the term DCP is known. In the case of the Favignana stalactite, the age of 806 BP (calibrated 705 cal BP), that is, of the sample S3 would become 478 BP (calibrated 518 cal BP) with a dead carbon percentage of 4%. Even a percentage of DCP of 10% would be enough to make the sample modern. In other words, if the DCP percentage of "dead" carbon in the cave were 10%, the sample would correspond to the present. This is obviously not reasonable, also because the stalactite is submerged. This suggests that the effect of carbon dead is very low (or negligible) in the studied cave. After all, the dating of 705 BP, without considering dead carbon effects, fits perfectly with the curve and this cannot be considered a coincidence. We took into account this question, but the analysis of datings leads us to think that this effect is completely negligible.

In Figure 12, the stalactite age with different ice models for Favignana (see caption figure 10 and Table 3)

Preprints (www.preprints.org) | NOT PEER-REVIEWED | Posted: 6 May 2021 doi:10.20944/preprints202105.0100.v1

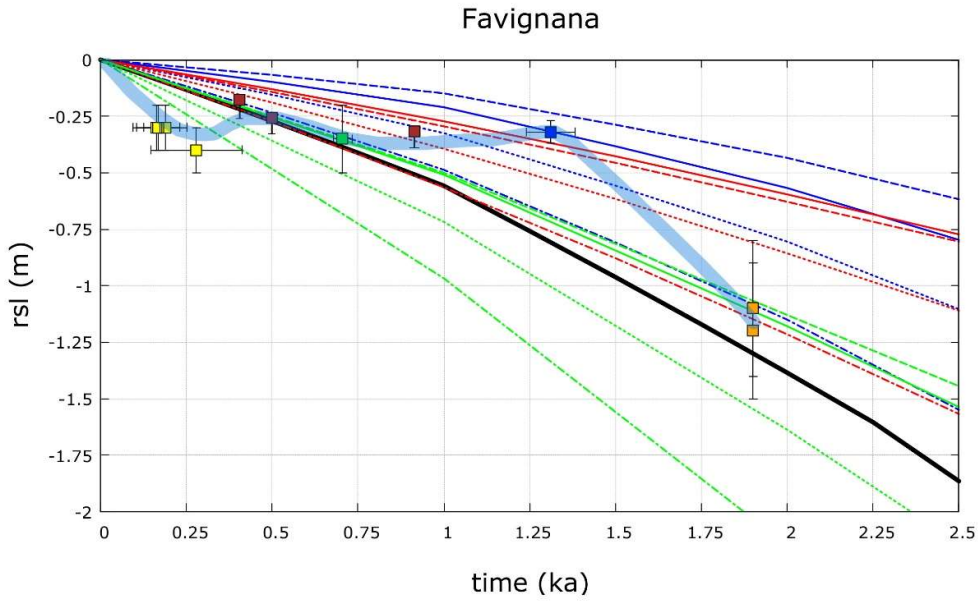

Figure 12 Last 2 ka BP sea level history using the phreatic speleothem (blu square), serpulids overgrowth (green square) sampled at Favignana compared with: 1) different sea ice models (See caption of Figure 11 for ice model); 2) a fishtank form Sorrento (Aucelli et al., 2017, light brown squares); 3) arcaheological markers (brown squares) from the S. Nicola cathedral (Pagliarulo et al., 2013); 4) Vermetid reef from S.Vito lo Capo (see Table 4). The sea level change (blue) curve seem to intercept the Warm Medioeval Period and the Little Ice Age.

and other geomorphological and geoarchaeological markers of the same time range are compared. The Serpulid overgrowth dated back to 1395 cal BP yields quite above almost any curve. The phreatic speleothem dated back to 705 years is instead in agreement with the average of the curves. Then, we added, as shown in Figure 16, some archaeological and biological markers included in the 2 ka time range. For example a fishtank in Salerno at -1.4 m bsl aged back to 1.9 kyrs from [84]. At about -0.40 m we also

Preprints (www.preprints.org) | NOT PEER-REVIEWED | Posted: 6 May 2021 doi:10.20944/preprints202105.0100.v1

found a less precise marker (a walking surface of the basilica of San Nicola [81] at -0.32 m in Middle Ages. We also added, some radiocarbon ages on Vermetid reefs [65] at -0.3 m dated back to 169, 163, 189 years cal BP and another one at -0.4 cm dated back to 279 years cal BP. Even if we advance these hypotheses with few data, it would seem to notice a peak of the sl curve corresponding with the Medieval Warm Period between 900 and 1200 years AD and a cooling corresponding with the Little Ice Age between 1550 and 1900 years AD). This trend is in agreemen with what was also found in Israel by [80].

4.2 Ustica stalactite

The stalactite sampled at the present-day sea level is about 0.8 cm long, with a diameter ranging from 4 to 8 cm (Figure 4 c). As shown in Tables 2 and 3, this speleothem also covers a very narrow time range of about 900 to 1000 years (Figure 4 a). There is a high concretion rate which could surprise, given that we are in a volcanic area. But the Ustica lava contains many fragments of carbonate platform erupted together with the lava, and often these carbonate ouotcrops werefound within lava outcrops up to few dozen meters. In some cases oalso with a modern tidal notch [51]. The most recent portion of the speleothem is formed by large living serpulid tubes. In the portion, between the continental part and the living polychaete worms, a continental sediment showing a different color was observed (Figure 4 b) together with porosity and with polychaete tubes, sponges incorporated in the sediment, is clearly visible.

The mixed deposition of continental carbonate with serpulid tubes (Figure 5b) costituites a clear signal of positive and negative vertical coseismic movements. The radiocarbon age of this outer portion, shows older values (albeit in perfect stratigraphic order) with respect to the central part (Figure 5a) of the satalactite aged with U-Th. The last part is younger. Our explanation is that the dead carbon of the very ancient carbonate inclusions in the Ustica lava have altered the date but not the stratigraphic order. The average tide amplitude in Ustica of 36 cm (https: / /www.tide-forecast.com/) and the length of the sampled speleothem of about 85 cm (Figure 4 c), add a proof that over the last 1 ka the island of Ustica was affected by positive and negative cosismic events. This consideration is confirmed by the very recent coseismic movement described for the near, Grotta Segreta, with a coseismic uplift of 0.4 m due to the 1906 earthquake [51]. The studied stalactite indicates both positive and negative vertical movements, with a positive average component (uplift) that can be deduced from the altitude of the MIS 5.5 deposits containing *Persistrombus latus* at 35 m altitude [52] and by the presence of evident marine terraces raised on the lava, with an uplift rate ranging from 0.13 to 0.24 mm/yr [53] (see also Figure 5).

4.3 Caribbean and Japan speleothems

U-Th datings on the speleothems sampled at Bermuda, Bahamas and Yukatan caves (Figure 2, Table 1) provided detailed information on the timing, duration, and altitude of sea level highstands during late and middle Pleistocene.

4.3.1 MIS 2 - Holocene

[11] analyzed a peculiar speleothem that preserves 4 marine *hiati* between 10.9 e 58 kyrs cal BP. The region under consideration is considered to be tectonically stable and it is very unikely that GIA could have been responsible for these anomalous crustal and/or sea surface fluctuations.

[13] studies a cave on the island of Minami Daito in Japan, which was made of a beautiful phreatic overgrowth. The authors investigated the relationship between the highest POS level, which represents the maximum elevation reached by the palaeo-groundwater level and the observed modern highest peak. Regardless of a relevant local mean tide fluctuation of 1.5 m, the authors found that between 5.4 and 4.6 cal BP, the local sl reached a maxmimum highstand of ~ 35 cm during the mid-Holocene. This can be explained by the GIA-drivem ocean syphoning.

Preprints (www.preprints.org) | NOT PEER-REVIEWED | Posted: 6 May 2021 doi:10.20944/preprints202105.0100.v1

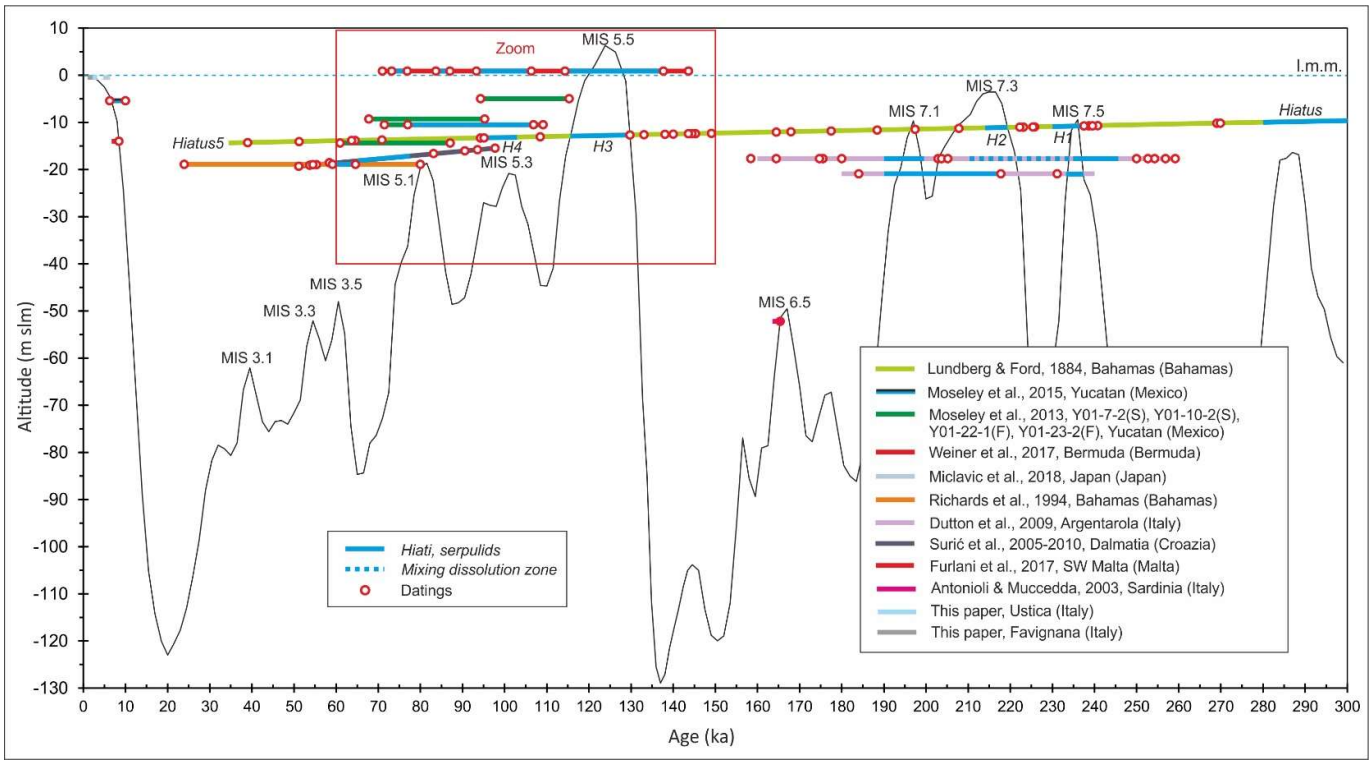

Figure 13 Predicted RSL curves for ICE-5G (red curves), ICE-6G (green curves) and ANICE-SELEN (blue curves) ice sheets models in combination with MVP 1-3 mantle viscosity profiles (solid, dashed and dotted, respectively) at each site and with respect to the measured elevations. a, Favignana. b, Yucatan. c, Bermuda. d, Bahamas.

4.3.2 MIS 3

Figures 13 and 14 show that the GB-89-25-5c speleothem that was sampled at an elevation of -18.1 m bsl in Bahamas [4] preserves a hiatus between 63.7 ± 1.7 kyrs and 58.5 ± 0.7 kyrs (MIS 3.5, Table 1 Figure 6). The lack of RSL data related to MIS 3.3 (and MIS 3 in general) make this a very unique and important indicator from a nearly tectonically stable area. Figure 13 shows that the global sea-level curve from [79] is characterized by a much lower highstand of -48 m bsl.

Our GIA predictions for the three ice sheets models and mantle viscosity profiles are characterized by lower RSL peaks at MIS 3 (Figure 9 a-c). Because the three ice sheets models are all somehow tuned to the $\delta^{18}O$ stack curve, we argue that their volumes might be biased towards larger values, while the speleothems here described might require a volume reduction throughout the MIS 3. The latter would, in fact, result in a much higher eustatic level. Interestingly, this is supported by the laters ice sheets model reconstruction from [85] that, for the MIS 3, provides a eustatic peak of ~28 m bsl. The authors used ice proximal glaciological and geological evidences to contrain the maximum extent of ice sheets through time and reconstruct the ice thickness by modelling the 2D ice profiles based on viscoplastic ice rheological flow law and 2D bottom shear stress. The model, therefore, is fully independent from far-field RSl observations and deep sea sea-level proxies.

4.3.3 MIS 5.1

The Yucatan speleothems do not record any hiatuses during the MIS 5.1 highstand, which therefore did not exceed the elevation of -14.6 m bsl [10]. Similarly, the DWBAH flowstone from Bahamas (corrected for vertical tectonics), does not show any evidence of local sea level higher than -13.5 m bsl (Figure 13). Hiatuses are also lacking in the GB-89-25-5c speleothem (Bahamas; [4]), which therefore limits the maximum highstand to -18.1 m bsl.

Preprints (www.preprints.org) | NOT PEER-REVIEWED | Posted: 6 May 2021 doi:10.20944/preprints202105.0100.v1

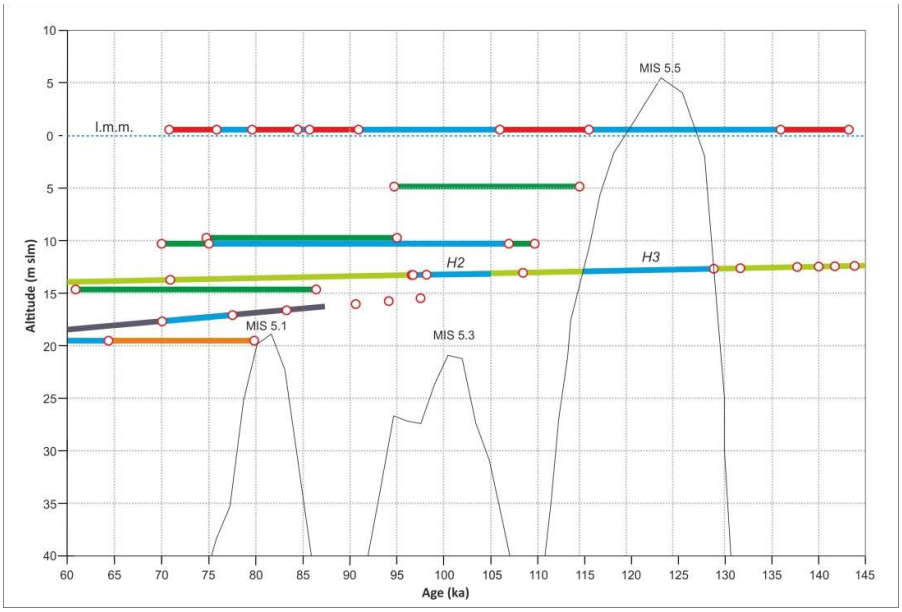

Figure 14 Zoom of Figure 13. Fine black line: global sea level curve reconstructed by [88].

Yucatan and Bahamas are in an intermediate-to-far-field position with respect to the ice sheet, where ice-loading related deformations and ocean syphoning might prevail (Figure 15). Our GIA-modulated RSL curves for Yucatan and Bahamas (see Figure 10 b,d) are all lower than the measured elevations (also corrected for tectonics). [9] explain the elevation of the MIS 5.1-5.3 hiatuses at Bermuda, sampled at +1.5 m (Table 1), as a consequence of the local GIA. The island, in fact, is considered tectonically stable but very

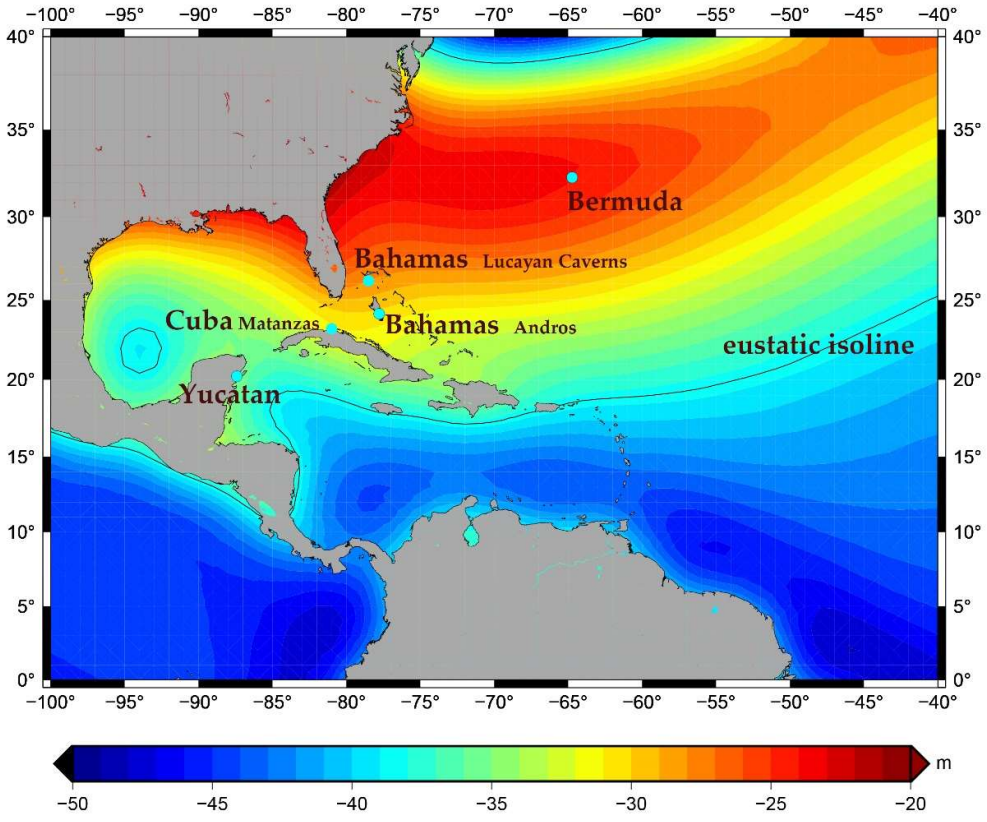

Figure 15. Predicted RSL elevation in the

Preprints (www.preprints.org) | NOT PEER-REVIEWED | Posted: 6 May 2021 doi:10.20944/preprints202105.0100.v1

Caribbean Sea during MIS 5.1 according to ANICE-SELEN and the MVP 3 mantle viscosity profile. The light blue dots indicate the location of the sites. The black isoline corresponds to the eustatic value (−38.5 m).

close to the peripheral forebulge that surrounded the North American ice sheet (see Figure 10 c and 15). Bermuda, therefore, is highly affected by the vertical motions of the forebulge, i.e. uplift during ice sheet expansion and subsidence during ice sheet retreat (Figure 15).

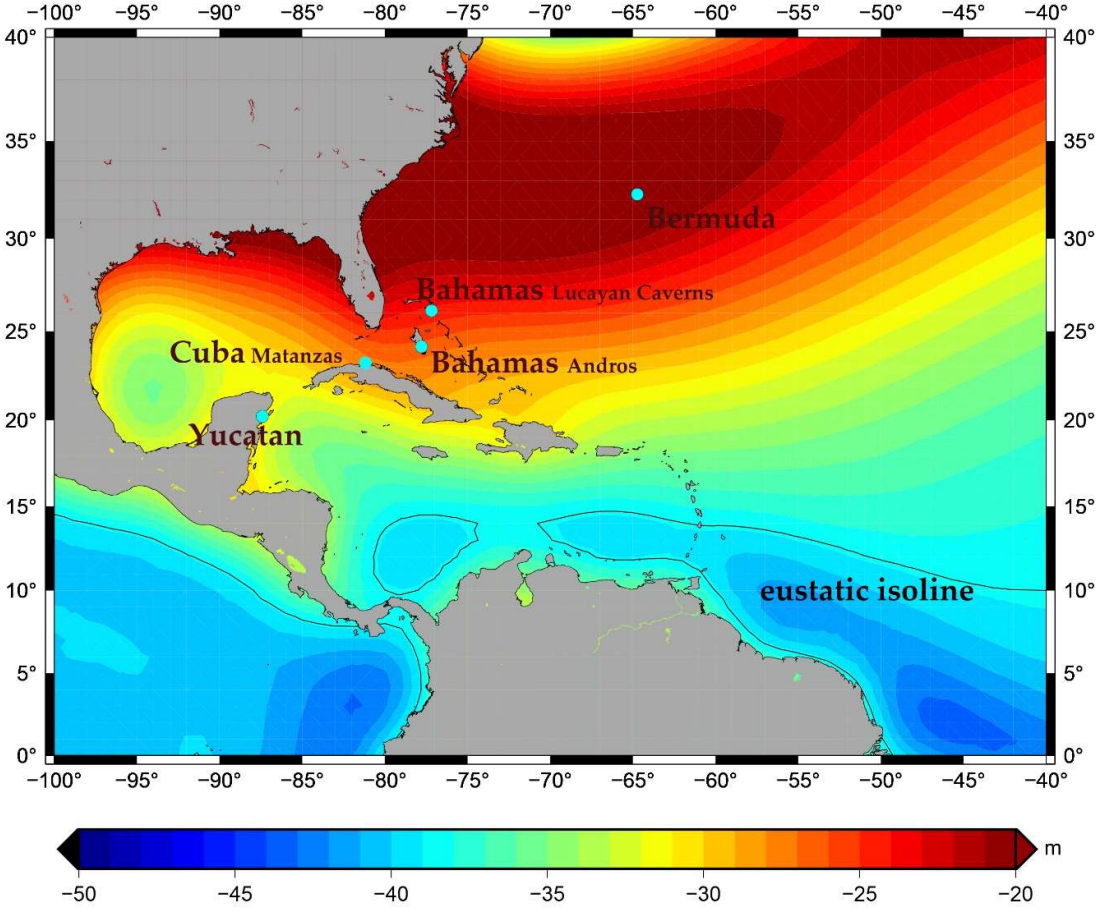

Preprints (www.preprints.org) | NOT PEER-REVIEWED | Posted: 6 May 2021 doi:10.20944/preprints202105.0100.v1

Figure 16 Predicted RSL elevation in the Caribbean Sea during MIS 5.3 according to ANICE-SELEN and the MVP 3 mantle viscosity profile. The light blue dots indicate the location of the sites. The black isoline corresponds to the eustatic value (-38.81 m).

Our highest MIS 5.1 sea-level prediction in Bermuda reach -18 m, while lower elevations of -25 and -20 m are predicted, respectively, at Yucatan and Bahamas (Figure 10 b,d). This confirms, indeed, that Bermuda is more affected by the GIA-related forebulge processes than Yucatan and Bahamas (Figure 15)

The elevations inferred from the Caribbean speleothems of Bahamas and Yucatan (-13.5 to -18.1 m) are somehow comparable that observed in the Mediterranean site of the Argentarola cave (-18.8 m) [6,86]. We argue that an elevation of -19 m could be representative of the intermediate-field areas such as the Caribbean and the Mediterranean Sea, in agreement with Linberg (1999) and [85].

Therefore, by removing the expected GIA contributions, we also hypothesize an eustatic elevation for the MIS 5.1 of approximately −17 m, obtained as average value between −18.8 and −13.5 m.

4.3.4 MIS 5.3

The speleothem from Bermuda which lyes at+1.5 m asl preserves several hiatuses and is likely affected by the forebulge processes (Figure 9 a-c, 10c and 16).

The DBWAH flowstone from Bahamas at -13.0 m bsl shows a MIS 5.3 hiatus that, again, cannot be explained with our GIA results.

A hiatus is recorded in Yucatan, where the sea level might have been higher than -11m after 109 ka, but lower than -5 m.

As it occurs with the MIS 5.1 elevations, our GIA predictions for the MIS 5.3 highstand cannot reach the observed elevations (Figure 9 a-c, 10 ab-d). Again, we argue that a reduction of ice sheets volumes is required to shift the eustatic value upwards.

We suggest a eustatic highstand between -12 and -6 m.

4.3.5 MIS 5.5

All the submerged speleothems from the Caribbean seashow hiati between -6 m bsl at 117 kyrs (Yucatan), -18.1 m bsl at 148 kyrs (Bahamas), at -14 at 134 kyrs of the flowstone DWBAH. The only difference is the timing of the transgression. In Bermuda the hiatus of MIS 5.5 is between 114 kyrs and 137 kyrs.

4.3.6 Middle Pleistocene

The only age oldest than MIS 5.5 was provided by the DWBAH flowstone [3,5] which contains 5 marine hiati (MIS 9, 7.5, 7.3, 5.5, 5.3)

We can provide some considerations on differences in tide amplitude between the Carribean sea and MS. Table 1 shows the maximum tide amplitudes in Bermuda and

 doi:10.20944/preprints202105.0100.v1

Bahamas of about 1.3 m and lower than 0.5 m in the other sites in the MS. Some corals used by some key studies, such as [87,88], used *Acropora palmata* with a depth range from -1 m bsl to -20 m bsl (as measured by F. Antonioli in Barbados). In our opinion the precision in elevation of the submerged speleothems is higher than corals. This is due to the fact that speleothems are precise indicators with respect to the mean sea level for tides lower than 0.5 m, (Table1).

5. Conclusions

Submerged speleothems can grow for significantly long temporal spans and, therefore, can record multiple intervals during which deposition stops and/or erosion takes over in response to sea-level highstands. The alternance of continental depostional layers and hiatuses or marine layers records, therefore, the long-term climat-related global ice-sheets fluctuations. In this review, we show that the use of submerged speleothems significantly contributed to constrain the short-term (Holocene) and long-term (Middle and mostly Late Pleistocene) sea level changes in the Caribbean, Japan and Mediterranean Sea.

The longest time span is recorded in the DWBHA flowstone [3] at Bahamas and covers the last 326 ka with 5 hiatuses recorded. The Bahamas speleothem GB-89-25-5 covers the time span between 80 and 24 ka and contains one hiatus.
At Bermuda, the QB speleothem covers the time span between 70 and 146 ka and records 4 *hiati*. Several speleothems from Yucatan [10] cover a time span ranging from 61 to 115 ka, with one evident hiatus. In the Mediterranean Sea, the ASI speleothem from Argentarola [86] covers the last 210 ka and records 4 hiatuses. The K-18 stalactite from Croatia [6,26] spans from 55 to 131 ka ka and contains 1 hiatus.

Overall, the discussed speleothems reflect the effects of the regionally-varying GIA signal, which shows up with its RSL fingerprints that stem from ice-sheets configurations and solid Earth response.

Holocene:

Continental, POS and marine overgrowth (serpulids) portions from submerged speleothems in Favignana (Mediterranean Sea) allow the construction of a sea level curve for the last 2000 years (Figure 12).

The Yucatan speleothems record 4 *hiati* between 10.8 e 4,6 ka, which suggesthigh-frequency sea-level fluctuations that might have been overimposed to the alocal falling sea-level in response to the GIA-driven ocean syphoning and continental levering (Mosely et al 2015).

Similarly, the phreatic speleothem from Minami Daito Island in Japan, records a mid Holocene sea-level highstand of 0.35 m, which is characteristic of the far-field Asian sites where the ocean syphoning process dominates tipico dei mari asiatici [13].

MIS 3:

The Bahamas elevation is -18.1, much higher than the typical global esustatic curves, but also higher than the observed value from the Mediterranean sites (-29 to -19 m). This might be due to the different GIA response of the two regions.

MIS 5.1:

 doi:10.20944/preprints202105.0100.v1

The presence and/or absence of hiatuses in the Bahamas and Mediterranean speleothems indicate a sea level between -13.5 and -19 m. The higher elevation at Bermuda is related to the GIA.

MIS 5.3:

The presence and/or absence of hiatuses suggest a eustatic sea level between -12 and -6 m. At Bermuda, the a MIS 5.3 exceeds the +1.5 m of elevation because of local GIA.

MIS 5.5:

All the speleothemes record hiatuses between 117 and 148 ka. In particular, the -6m elevation of the Yucatan speleothem, constrains the end of the MIS 5e local highstand. Similarly, the elevations of -18.1 and -14 m constrain, respectively at 148 and 134 ka, the local RSL rise at Bahamas before the actual MIS 5e highstand.

The maximum vertical differences between the GIA-modulated MIS 5.5 highstands from the different Caribbean sites, have been quantified on the order of ~8 m, typical of intermediate-field regions. In the Mediterranean Sea, instead, the vertical differences are less than 2.5 m, thus showing that this is an intermediate-to-far-field region [59].

Middle Pleistocene

MIS 7.1:
The flowstone at -14 m dos not record any hiatuses, while the three speleothems from the Argentarola cave (Figure 13) show a clearly visible Serpulid overgrowth.

MIS 7.2:
A clear highstand is recorded in the Argentarola cave. The sea level oscillated betweenn -18.5 -21 m, similarly to the global curve that reaches -27 m.

MIS 7.3:
The Bahamas flowstone at -14 m does not preserve any hiatuses. The Argentarola stalagmite shows marine conditions at -18.5 m, but the local sea leve did not exceed -18.0 m -18. Therefore, we argue that the global sea level was between 14 and 18 m b.m.s.l.

MIS 7.5:
The observed highstand in the DWBAH flowstone is certainly higher than -18 m and presumably lower than -12 m, thus in agreement again with the global curve.

We show that the GIA-driven RSL variability at the sites under consideration increases during the interstadials and glacials. We arguet that this stems from the contribution for the ice-loading-induced crustal and geoidal deformations, which maintain strong spatial RSL gradients.

Author Contributions: For research articles with several authors, a short paragraph specifying their individual contributions must be provided. The following statements should be used "Conceptualization, F.A., P.M., P.S.; methodology, P.M., P.S. S.F.; formal analysis, G.Q, L.C., P.M.; investigation, F.A, S.F., V.LP., V.V., J.C., M.G.; writing—original draft preparation, F.A., P.S., P.M.; F.M., M, G., writing-review and editing, S.F.,P.M.,P.S. All authors have read and agreed to the published version of the manuscript." Please turn to the CRediT taxonomy for the term explanation. Authorship must be limited to those who have contributed substantially to the work reported.

Funding: This research received no external funding

Data Availability Statement: In this section, please provide details regarding where data supporting reported results can be found, including links to publicly archived datasets analyzed or generated during the study. Please refer to suggested Data Availability Statements in section "MDPI Research Data Policies" at https://www.mdpi.com/ethics. You might choose to exclude this statement if the study did not report any data.

Acknowledgments: we thanks Joyce Lundberg, Yusuke Yokoyama, Blaz Miklavic, Gina Moseley, David Richards, for sending photos. AMP Egadi, Alice Busetti for help in sampling speleothem at Favignana. AMP Ustica and Salvatore Livreri Console.

Conflicts of Interest: The authors declare no conflict of interest.

REFERENCES

1. Spalding, R.F.; Mathews, T.D. Stalagmites from caves in the Bahamas: Indicators of low sea level stand. *Quat. Res.* **1972**, *2*, 470–472, doi:10.1016/0033-5894(72)90085-3.

2. Ginés, A.; Ginés, J. Consideraciones sobre los mecanismos de fosilización de la "Cova de Sa Bassa Blanca" y su paralelismo con formaciones marinas del Cuaternario. *Bolletí la Soc. d'Història Nat. les Balear.* **1974**, *19*, 11–28.

3. Li, W.X.; Lundberg, J.; Dickin, A.P.; Ford, D.C.; Schwarcz, H.P.; McNutt, R.; Williams, D. High-precision mass-spectrometric uranium-series dating of cave deposits and implications for palaeoclimate studies. *Nature* **1989**, *339*, 534–536, doi:10.1038/339534a0.

4. Richards, D.A.; Smart, P.L.; Lawrence Edwards, R. Maximum sea levels for the last glacial period from U-series ages of submerged speleothems. *Nature* **1994**, *367*, 357–360, doi:10.1038/367357a0.

5. Lundberg, J.; Ford, D.C. Late pleistocene sea level change in the Bahamas from mass spectrometric U-series dating of submerged speleothem. *Quat. Sci. Rev.* **1994**, *13*, 1–14, doi:10.1016/0277-3791(94)90121-X.

6. Antonioli, F.; Furlani, S.; Montagna, P.; Stocchi, P. The Use of Submerged Speleothems for Sea Level Studies in the Mediterranean Sea: A New Perspective Using Glacial Isostatic Adjustment (GIA). *Geosci.* 2021, *11*.

7. Gascoyne, M.; Benjamin, G.J.; Schwarcz, H.P.; Ford, D.C. Sea-level lowering during the Illinoian glaciation: Evidence from a Bahama "blue hole." *Science (80-.).* **1979**, *205*, 806–808, doi:10.1126/science.205.4408.806.

8. Harmon, R.S.; Land, L.S.; Mitterer, R.M.; Garrett, P.; Schwarcz, H.P.; Larson, G.J. Bermuda sea level during the last interglacial. *Nature* **1981**, *289*, 481–483, doi:10.1038/289481a0.

9. Wainer, K.A.I.; Rowe, M.P.; Thomas, A.L.; Mason, A.J.; Williams, B.; Tamisiea, M.E.; Williams, F.H.; Düsterhus, A.; Henderson, G.M. Speleothem evidence for MIS 5c and 5a sea level above modern level at Bermuda. *Earth Planet. Sci. Lett.* **2017**, *457*, 325–334, doi:https://doi.org/10.1016/j.epsl.2016.10.005.

10. Moseley, G.; Smart, P.L.; Richards, D.A.; Hoffmann, D.L. Speleothem constraints on marine isotope stage (MIS) 5 relative sea levels, Yucatan Peninsula, Mexico. *J. Quat. Sci.* **2013**, *28*, 293–300, doi:10.1002/jqs.2613.

11. Moseley, G.E.; Richards, D.A.; Smart, P.L.; Standish, C.D.; Hoffmann, D.L.; ten Hove, H.; Vinn, O. Early–middle Holocene relative sea-level oscillation events recorded in a submerged speleothem from the Yucatán Peninsula, Mexico. *The Holocene* **2015**, *25*, 1511–1521, doi:10.1177/0959683615585832.

12. De Waele, J.; D'Angeli, I.M.; Bontognali, T.; Tuccimei, P.; Scholz, D.; Jochum, K.P.; Columbu, A.; Bernasconi, S.M.; Fornós, J.J.; Grau González, E.R.; et al. Speleothems in a north Cuban cave register sea-level changes and Pleistocene uplift rates. *Earth Surf. Process. Landforms* **2018**, *43*, 2313–2326, doi:10.1002/esp.4393.

13. Miklavič, B.; Yokoyama, Y.; Urata, K.; Miyairi, Y.; Kan, H. Holocene relative sea level history from phreatic overgrowths on speleothems (POS) on Minami Daito Island, Northern Philippine Sea. *Quat. Int.* **2018**, *471*, 359–368, doi:https://doi.org/10.1016/j.quaint.2017.09.032.

14. Van Hengstum, P.J.; Richards, D.A.; Onac, B.P.; Dorale, J.A. Coastal caves and sinkholes. In *Handbook of Sea-Level Research*; John Wiley & Sons, Ltd: Chichester, UK, 2015; pp. 83–103.

15. Dumitru, O.A.; Polyak, V.J.; Asmerom, Y.; Onac, B.P. Last Interglacial (sensu latu, ~130 to 75 ka) sea level history from cave deposits: a global standardized database. *Earth Syst. Sci. Data Discuss.* **2020**, *2020*, 1–25, doi:10.5194/essd-2020-387.

16. Mylroie, J.E.; Lace, M.J.; Kambesis, P.N.; Mylroie, J.R. Karst Processes and Estuarine Coastlines BT - Encyclopedia of Estuaries. In; Kennish, M.J., Ed.; Springer Netherlands: Dordrecht, 2016; pp. 373–380 ISBN 978-94-017-8801-4.

17. Emery, K.O.; Uchupi, E. Western North Atlantic Ocean: Topography, Rocks, Structure, Water, Life, and Sediments 1972.

18. Smart, P.L.; Beddows, P.A.; Coke, J.; Doerr, S.; Smith, S.; Whitaker, F.F. Cave development on the Caribbean coast of the Yucatan Peninsula, Quintana Roo, Mexico. In *Perspectives on Karst Geomorphology, Hydrology, and Geochemistry - A Tribute Volume to Derek C. Ford and William B. White*; Harmon, R.S., Wicks, C.M., Eds.; Geological Society of America, 2006; Vol. 404, p. 0 ISBN 9780813724041.

19. De Waele, J.; D'Angeli, I.M.; Tisato, N.; Tuccimei, P.; Soligo, M.; Ginés, J.; Ginés, A.; Fornós, J.J.; Villa, I.M.; Grau González, E.R.; et al. Coastal uplift rate at Matanzas (Cuba) inferred from MIS5e phreatic overgrowths on speleothems. *Terra Nov.* **2017**, *29*, 98–105, doi:https://doi.org/10.1111/ter.12253.

20. Cabrera, M.; Penalver, L.L. Contribuci_on a la estratigraf_ıa de los dep_ositos Cuaternarios de Cuba. *Cuaternario y Geomorfol. Rev. la Soc. Esp. Geomorfol. y Asoc. Esp. para el Estud. del Cuaternario* **2001**, *15*, 37–49.

21. Hearty, P.J.; Kindler, P. The Stratigraphy and Surficial Geology of New Providence and Surrounding Islands, Bahamas. *J. Coast. Res.* **1997**, *13*, 798–812.

22. Vacher, L.; Quinn, T. *Geology and hydrogeology of carbonate islands*; Elsevier Science, 1997; ISBN 9780080532479.

23. Ohde, S.; Elderfield, H. Strontium isotope stratigraphy of Kita-daito-jima Atoll, North Philippine Sea: implications for Neogene sea-level change and tectonic history. *Earth Planet. Sci. Lett.* **1992**, *113*, 473–486, doi:https://doi.org/10.1016/0012-821X(92)90125-F.

24. Tam, E.; Yokoyama, Y. A review of MIS 5e sea-level proxies around Japan. *Earth Syst. Sci. Data* **2021**, *13*, 1477–1497, doi:10.5194/essd-13-1477-2021.

25. Stocchi, P.; Antonioli, F.; Montagna, P.; Pepe, F.; Lo Presti, V.; Caruso, A.; Corradino, M.; Dardanelli, G.; Renda, P.; Frank, N.; et al. A stalactite record of four relative sea-level highstands during the Middle Pleistocene Transition. *Quat. Sci. Rev.* **2017**, *173*, 92–100, doi:10.1016/j.quascirev.2017.08.008.

26. Surić, M.; Richards, D.A.; Hoffmann, D.L.; Tibljaš, D.; Juračić, M. Sea-level change during MIS 5a based on submerged speleothems from the eastern Adriatic Sea (Croatia). *Mar. Geol.* **2009**, *262*, 62–67, doi:10.1016/j.margeo.2009.03.005.

27. Vesica, P.L.; Tuccimei, P.; Turi, B.; Fornós, J.J.; Ginés, A.; Ginés, J. Late Pleistocene Paleoclimates and sea-level change in the Mediterranean as inferred from stable isotope and U-series studies of overgrowths on speleothems, Mallorca, Spain. *Quat. Sci. Rev.* **2000**, *19*, 865–879, doi:10.1016/S0277-3791(99)00026-8.

28. Tuccimei, P.; Soligo, M.; Ginés, J.; Ginés, A.; Fornós, J.; Kramers, J.; Villa, I.M. Constraining Holocene sea levels using U-Th ages of phreatic overgrowths on speleothems from coastal caves in Mallorca (Western Mediterranean). *Earth Surf. Process. Landforms* **2010**, *35*, n/a-n/a, doi:10.1002/esp.1955.

29. Dorale, J.A.; Onac, B.P.; Fornós, J.J.; Ginés, J.; Ginés, A.; Tuccimei, P.; Peate, D.W. Sea-level highstand 81, 000 years ago in mallorca. *Science (80-.).* **2010**, *327*, 860–863, doi:10.1126/science.1181725.

30. Polyak, V.J.; Onac, B.P.; Fornós, J.J.; Hay, C.; Asmerom, Y.; Dorale, J.A.; Ginés, J.; Tuccimei, P.; Ginés, A. A highly resolved record of relative sea level in the western Mediterranean Sea during the last interglacial period. *Nat. Geosci.* **2018**, *11*, 860–864, doi:10.1038/s41561-018-0222-5.

31. Lucia, G.; Polyak, V.J.; Ginés, J.; Fornòs, J.J.; Ginés, A.; Asmerom, Y.; Onac, B.P. Chronology of Middle Pleistocene Coastal Karst Evolution and Relative Sea-Level Changes in Mallorca. *J. Coast. Res.* **2020**, *in press*, doi:10.2112/jcoastres-d-20-00082.1.

32. Alessio, M.; Allegri, L.; Antonioli, F.; Belluomini, G.; Ferranti, L.; Improta, S.; Manfra, L.; Proposito, A. Risultati preliminari relativi alla datazione di speleotemi sommersi nelle fasce costiere del Tirreno centrale. *G. di Geol.* **1992**, *54*, 165–194.

33. Dutton, A.; Scicchitano, G.; Monaco, C.; Desmarchelier, J.M.; Antonioli, F.; Lambeck, K.; Esat, T.M.; Fifield, L.K.; McCulloch, M.T.; Mortimer, G. Uplift rates defined by U-series and 14C ages of serpulid-encrusted speleothems from submerged caves near Siracusa, Sicily (Italy). *Quat. Geochronol.* **2009**, *4*, 2–10, doi:10.1016/j.quageo.2008.06.003.

34. Dutton, A.; Bard, E.; Antonioli, F.; Esat, T.M.; Lambeck, K.; McCulloch, M.T. Phasing and amplitude of sea-level and climate change during the penultimate interglacial. *Nat. Geosci.* **2009**, *2*, 355–359, doi:10.1038/ngeo470.

35. Surić, M.; Lončarić, R.; Lončar, N. Submerged caves of Croatia: Distribution, classification and origin. *Environ. Earth Sci.* **2010**, *61*, 1473–1480, doi:10.1007/s12665-010-0463-0.

36. Furlani, S.; Antonioli, F.; Gambin, T.; Biolchi, S.; Formosa, S.; Lo Presti, V.; Mantovani, M.; Anzidei, M.; Calcagnile, L.; Quarta, G. Submerged speleothem in Malta indicates tectonic stability throughout the Holocene. *The Holocene* **2018**, *28*, 1588–1597, doi:10.1177/0959683618782613.

37. Alessio, M.; Allegri, L.; Antonioli, F.; Belluomini, G.; Impronta, S.; Manfra, L.; Preite, M. La curva di risalita del Mare Tirreno negli ultimi 43 ka ricavata da datazioni su speleotemi sommersi e dati archeologici. *Mem. Descr. del Serv. Geol. Naz.* **1994**, *52*, 261–276.

38. Antonioli, F.; Bard, E.; Potter, E.K.; Silenzi, S.; Improta, S. 215-ka history of sea-level oscillations from marine and continental layers in Argentarola Cave speleothems (Italy). *Glob. Planet. Change* **2004**, *43*, 57–78, doi:10.1016/j.gloplacha.2004.02.004.

39. Furlani, S.; Pappalardo, M.; Gómez-Pujol, L.; Chelli, A. The rock coast of the Mediterranean and Black seas. *Geol. Soc. Mem.* **2014**, *40*, 89–123, doi:10.1144/M40.7.

40. Rohling, E.J.; Abu-Zied, R.; Casford, C.S.L.; Hayes, A.; Hoogakker, B.A.A. The Mediterranean Sea: Present and Past. In *Physical Geography of the Mediterranean Basin*; Oxford University Press, Oxford, 2009 ISBN 978-0-19-926803-0.

41. Giese, P.; Morelli, C. La struttura della crosta terrestre in Italia. *Accad. Naz. Lincei* **1973**, *183*, 317–362.

42. Sulli, A.; Zizzo, E.; Spatola, D.; Gasparo Morticelli, M.; Agate, M.; Lo Iacono, C.; Gargano, F.; Pepe, F.; Ciaccio, G. Growth and geomorphic evolution of the Ustica volcanic complex at the Africa-Europe plate margin (Tyrrhenian Sea). *Geomorphology* **2021**, *374*, 107526, doi:https://doi.org/10.1016/j.geomorph.2020.107526.

43. Bousquet, J.C.; Lanzafame, E.G. Evidence of north-south compression at Ustica (southern Tyrrhenian Sea) 1992, 1–6.

44. Bonomo, R.; Ricci, V. Application of unconformity-bounded stratigraphic (UBS) units to the geological survey of the volcanic island Ustica (Italy). In *Stratigraphy and Geology of Volcanic Areas*; Groppelli, G., Viereck-Goette, L., Eds.; Geological Society of America, 2010; Vol. 464, p. 0 ISBN 9780813724645.

45. Romano, R.; Sturiale, C. L'isola di Ustica: Studio Geo-vulcanologico e Magmatologico. *Riv. Miner. Sicil.* **1971**, *22*, 3–61.

46. De Vita, S. Assetto Geologico-Strutturale ed Evoluzione Vulcanologica Dell'isola di Ustica (Stratigrafia, Tettonica e Meccanismi Eruttivi), Università degli Studi di Napoli Federico II, 1993.

47. de Vita, S.; Guzzetta, G.; Orsi, G. Deformational features of the Ustica volcanic island in the Southern Tyrrhenian Sea (Italy). *Terra Nov.* **1995**, *7*, 623–629, doi:https://doi.org/10.1111/j.1365-3121.1995.tb00711.x.

48. Peccerillo, A. *Plio-Quaternary Volcanism in Italy*; Springer, Berlin, Heidelberg, 2005; ISBN 978-3-540-25885-8.

49. de Vita, S.; Laurenzi, M.A.; Orsi, G.; Voltaggio, M. APPLICATION OF 40Ar/39Ar AND 230Th DATING METHODS TO THE CHRONOSTRATIGRAPHY OF QUATERNARY BASALTIC VOLCANIC AREAS: THE USTICA ISLAND CASE HISTORY. *Quat. Int.* **1998**, *47–48*, 117–127, doi:https://doi.org/10.1016/S1040-6182(97)00077-3.

50. Cinque, A.; Civetta, L.; Orsi, G.; Peccerillo, A. Geology and geochemistry of the island of Ustica (Southern Tyrrhenian Sea). *Boll. Soc. Ital. Miner. Pet.* **1998**, *43*, 987–1002.

51. Furlani, S.; Antonioli, F.; Cavallaro, D.; Chirco, P.; Caldareri, F.; Martin, F.F.; Morticelli, M.G.; Monaco, C.; Sulli, A.; Quarta, G.; et al. Tidal notches, coastal landforms and relative sea-level changes during the Late Quaternary at Ustica Island (Tyrrhenian Sea, Italy). *Geomorphology* **2017**, *299*, 94–106, doi:https://doi.org/10.1016/j.geomorph.2017.10.004.

52. de Vita, S.; Foresta Martin, F. The palaeogeographic setting and the local environmental impact of the 130 ka Falconiera tuff-cone eruption (Ustica island, Italy). *Ann. Geophys. Vol 60, No 2 (2017)DO - 10.4401/ag-7113* **2017**.

53. De Vita, S.; Orsi, G. I terrazzi marini dell'isola di Ustica (Mar Tirreno Meridionale, Italia). *Mem. Descr. Cart. Geol. It.* **1994**, *52*, 405–406.

54. Incandela, A. Deformazioni neogeniche nelle Isole di Favignana e Levanzo (Isole Egadi). *Mem. Soc. Geol. It.* **1996**, *51*, 129–135.

55. Abate, B.; Incandela, A.; Renda, P. Carta Geologica delle Isole di Favignana e Levanzo 1997.

56. Lo Presti, V.; Antonioli, F.; Palombo, M.R.; Agnesi, V.; Biolchi, S.; Calcagnile, L.; Di Patti, C.; Donati, S.; Furlani, S.; Merizzi, J.; et al. Palaeogeographical evolution of the Egadi Islands (western Sicily, Italy). Implications for late Pleistocene and early Holocene sea crossings by humans and other mammals in the western Mediterranean. *Earth-Science Rev.* **2019**, *194*, 160–181, doi:https://doi.org/10.1016/j.earscirev.2019.04.027.

57. Hearty, P.J.; Miller, G.H.; Stearns, C.E.; Szabo, B.J. Aminostratigraphy of Quaternary shorelines in the Mediterranean basin. *Geol. Soc. Am. Bull.* **1986**, *97*, 850–858, doi:10.1130/0016-7606(1986)97<850:AOQSIT>2.0.CO;2.

58. Antonioli, F.; Cremona, G.; Immordino, F.; Puglisi, C.; Romagnoli, C.; Silenzi, S.; Valpreda, E.; Verrubbi, V. New data on the Holocenic sea-level rise in NW Sicily (Central Mediterranean Sea). *Glob. Planet. Change* **2002**, *34*, 121–140, doi:10.1016/S0921-8181(02)00109-1.

59. Antonioli, F.; Ferranti, L.; Stocchi, P.; Deiana, G.; Lo Presti, V.; Furlani, S.; Marino, C.; Orru, P.; Scicchitano, G.; Trainito, E.; et al. Morphometry and elevation of the last interglacial tidal notches in tectonically stable coasts of the Mediterranean Sea. *Earth-Science Rev.* 2018, *185*, 600–623.

60. Pons-Branchu, E.; Douville, E.; Roy-Barman, M.; Dumont, E.; Branchu, P.; Thil, F.; Frank, N.; Bordier, L.; Borst, W. A geochemical perspective on Parisian urban history based on U-Th dating, laminae counting and yttrium and REE concentrations of recent carbonates in underground aqueducts. *Quat. Geochronol.* **2014**, *24*, 44–53, doi:10.1016/j.quageo.2014.08.001.

61. Ludwig, K.R.; Titterington, D.M. Calculation of 230Th U isochrons, ages, and errors. *Geochim. Cosmochim. Acta* **1994**, *58*, 5031–5042, doi:10.1016/0016-7037(94)90229-1.

62. Cheng, H.; Lawrence Edwards, R.; Shen, C.C.; Polyak, V.J.; Asmerom, Y.; Woodhead, J.; Hellstrom, J.; Wang, Y.; Kong, X.; Spötl, C.; et al. Improvements in 230Th dating, 230Th and 234U half-life values, and U-Th isotopic measurements by multi-collector inductively coupled plasma mass spectrometry. *Earth Planet. Sci. Lett.* **2013**, *371–372*, 82–91, doi:10.1016/j.epsl.2013.04.006.

63. Jaffey, A.H.; Flynn, K.F.; Glendenin, L.E.; Bentley, W.C.; Essling, A.M. Precision measurement of half-lives and specific activities of U235 and U238. *Phys. Rev. C* **1971**, *4*, 1889–1906, doi:10.1103/PhysRevC.4.1889.

64. Hans Wedepohl, K. The composition of the continental crust. *Geochim. Cosmochim. Acta* **1995**, *59*, 1217–1232, doi:10.1016/0016-7037(95)00038-2.

65. Antonioli, F.; Chemello, R.; Improta, S.; Riggio, S. Dendropoma lower intertidal reef formations and their palaeoclimatological significance, NW Sicily. *Mar. Geol.* **1999**, *161*, 155–170, doi:https://doi.org/10.1016/S0025-3227(99)00038-9.

66. Reimer, P.J.; Austin, W.E.N.; Bard, E.; Bayliss, A.; Blackwell, P.G.; Bronk Ramsey, C.; Butzin, M.; Cheng, H.; Edwards, R.L.; Friedrich, M.; et al. The IntCal20 Northern Hemisphere Radiocarbon Age Calibration Curve (0-55 cal kBP). *Radiocarbon* **2020**, *62*, 725–757, doi:10.1017/RDC.2020.41.

67. Calcagnile, L.; Maruccio, L.; Scrimieri, L.; delle Side, D.; Braione, E.; D'Elia, M.; Quarta, G. Development and application of facilities at the Centre for Applied Physics, Dating and Diagnostics (CEDAD) at the University of Salento during the last 15 years. *Nucl. Instruments Methods Phys. Res. Sect. B Beam Interact. with Mater. Atoms* **2019**, *456*, 252–256, doi:https://doi.org/10.1016/j.nimb.2019.03.031.

68. Heaton, T.J.; Köhler, P.; Butzin, M.; Bard, E.; Reimer, R.W.; Austin, W.E.N.; Bronk Ramsey, C.; Grootes, P.M.; Hughen, K.A.; Kromer, B.; et al. Marine20—The Marine Radiocarbon Age Calibration Curve (0–55,000 cal BP). *Radiocarbon* **2020**, *62*, 779–820, doi:DOI: 10.1017/RDC.2020.68.

69. Siani, G.; Paterne, M.; Arnold, M.; Bard, E.; Métivier, B.; Tisnerat, N.; Bassinot, F. Radiocarbon Reservoir Ages in the Mediterranean Sea and Black Sea. *Radiocarbon* **2000**, *42*, 271–280, doi:DOI: 10.1017/S0033822200059075.

70. Farrell, W.E.; Clark, J.A. On Postglacial Sea Level. *Geophys. J. R. Astron. Soc.* **2007**, *46*, 647–667, doi:10.1111/j.1365-246X.1976.tb01252.x.

71. Spada, G.; Stocchi, P. SELEN: A Fortran 90 program for solving the "sea-level equation." *Comput. Geosci.* **2007**, *33*, 538–562, doi:10.1016/j.cageo.2006.08.006.

72. Stocchi, P.; Vacchi, M.; Lorscheid, T.; de Boer, B.; Simms, A.R.; van de Wal, R.S.W.; Vermeersen, B.L.A.; Pappalardo, M.; Rovere, A. MIS 5e relative sea-level changes in the Mediterranean Sea: Contribution of isostatic disequilibrium. *Quat. Sci. Rev.* **2018**, *185*, 122–134, doi:10.1016/j.quascirev.2018.01.004.

73. Peltier, W.R. Global glacial isostasy and the surface of the ice-age Earth: the ICE-5G (VM2) model and GRACE. *Annu. Rev. Earth Planet. Sci.* **2004**, *32*, 111–149, doi:10.1146/annurev.earth.32.082503.144359.

74. Lisiecki, L.E.; Raymo, M.E. A Pliocene-Pleistocene stack of 57 globally distributed benthic δ 18O records. *Paleoceanography* **2005**, *20*, 1–17, doi:10.1029/2004PA001071.

75. Argus, D.F.; Peltier, W.R.; Drummond, R.; Moore, A.W. The Antarctica component of postglacial rebound model ICE-6G_C (VM5a) based on GPS positioning, exposure age dating of ice thicknesses, and relative sea level histories. *Geophys. J. Int.* **2014**, *198*, 537–563, doi:10.1093/gji/ggu140.

76. de Boer, B.; Stocchi, P.; van de Wal, R.S.W. A fully coupled 3-D ice-sheet–sea-level model: algorithm and applications. *Geosci. Model Dev.* **2014**, *7*, 2141–2156, doi:10.5194/gmd-7-2141-2014.

77. de Boer, B.; Stocchi, P.; Whitehouse, P.L.; van de Wal, R.S.W. Current state and future perspectives on coupled ice-sheet – sea-level modelling. *Quat. Sci. Rev.* 2017, *169*, 13–28.

78. Blanchon, P.; Eisenhauer, A.; Fietzke, J.; Liebetrau, V. Rapid sea-level rise and reef back-stepping at the close of the last interglacial highstand. *Nature* **2009**, *458*, 881–884, doi:10.1038/nature07933.

79. Waelbroeck, C.; Labeyrie, L.; Michel, E.; Duplessy, J.C.; McManus, J.F.; Lambeck, K.; Balbon, E.; Labracherie, M. Sea-level and deep water temperature changes derived from benthic foraminifera isotopic records. *Quat. Sci. Rev.* **2002**, *21*, 295–305, doi:10.1016/S0277-3791(01)00101-9.

80. Toker, E.; Sivan, D.; Stern, E.; Shirman, B.; Tsimplis, M.; Spada, G. Evidence for centennial scale sea level variability during the Medieval Climate Optimum (Crusader Period) in Israel, eastern Mediterranean. *Earth Planet. Sci. Lett.* **2012**, *315–316*, 51–61, doi:https://doi.org/10.1016/j.epsl.2011.07.019.

81. Pagliarulo, R.; Antonioli, F.; Anzidei, M. Sea level changes since the Middle Ages along the coast of the Adriatic Sea: The case of St. Nicholas Basilica, Bari, Southern Italy. *Quat. Int.* **2013**, *288*, 139–145, doi:https://doi.org/10.1016/j.quaint.2012.01.011.

82. Lambeck, K.; Antonioli, F.; Anzidei, M.; Ferranti, L.; Leoni, G.; Scicchitano, G.; Silenzi, S. Sea level change along the Italian coast during the Holocene and projections for the future. *Quat. Int.* **2011**, *232*, 250–257, doi:10.1016/j.quaint.2010.04.026.

83. Antonioli, F.; Silenzi, S.; Frisia, S. Tyrrhenian Holocene palaeoclimate trends from spelean serpulids. *Quat. Sci. Rev.* **2001**, *20*, 1661–1670, doi:10.1016/S0277-3791(01)00012-9.

84. Aucelli, P.; Cinque, A.; Mattei, G.; Pappone, G. Historical sea level changes and effects on the coasts of Sorrento Peninsula (Gulf of Naples): New constrains from recent geoarchaeological investigations. *Palaeogeogr. Palaeoclimatol. Palaeoecol.* **2016**, *463*, 112–125, doi:https://doi.org/10.1016/j.palaeo.2016.09.022.

85. Gowan, E.; Rovere, A.; Ryan, D.; Richiano, S.; Montes, A.; Pappalardo, M.; Aguirre, M. Last interglacial (MIS 5e) sea-level proxies in southeastern South America. *Earth Syst. Sci. Data Discuss.* **2020**, 1–40, doi:10.5194/essd-2020-247.

86. Bard, E.; Antonioli, F.; Silenzi, S. Sea-level during the penultimate interglacial period based on a submerged stalagmite from Argentarola Cave (Italy). *Earth Planet. Sci. Lett.* **2002**, *196*, 135–146, doi:10.1016/S0012-821X(01)00600-8.

87. Bard, E.; Hamelin, B.; Fairbanks, R.G.; Zindler, A.; Mathieu, G.; Arnold, M. U/Th and 14C ages of corals from Barbados and their use for calibrating the 14C time scale beyond 9000 years B.P. *Nucl. Inst. Methods Phys. Res. B* **1990**, *52*, 461–468, doi:10.1016/0168-583X(90)90458-7.

88. Blanchon, P.; Shaw, J. Reef drowning during the last deglaciation: Evidence for catastrophic sea-level rise and ice-sheet collapse. *Geology* **1995**, *23*, 4–8, doi:10.1130/0091-7613(1995)023<0004:RDDTLD>2.3.CO;2.

 doi:10.20944/preprints202105.0100.v1